https://doi.org/10.5194/egusphere-2025-6433
Preprint. Discussion started: 21 April 2026

The Mechanisms Behind Triggering the 2021-2022 South Alboran Seismic Swarm: Constrains from Combined Catalogues, Relocation and Spatiotemporal Analysis

Hamza Akka[1,2], Alexis Rigo[2], Abdelilah Tahayt[1]

[1]R&D in Applied Geosciences Laboratory, FSTT Abdelmalek Essaadi University, Tetouan, 91000, Morocco
[2]Laboratoir de Geologie, ENS PSL, CNRS, Paris, France

Correspondence to: Akka Hamza (hamza.akka@etu.uae.ac.ma)

Abstract. The Alboran system reflects the interplay of slow Nubia–Iberia convergence, inherited structures, and ongoing lithospheric attenuation. Earthquake occurrence mainly tracks active crustal fault networks that partition the oblique plate motion into strike-slip and extension. The 2021–2022 seismic swarm in the western Alboran Sea represents an exceptional episode characterized by complex temporal-spatial evolution, primarily influenced by fluid-driven processes interacting with inherited fault systems. We analyzed arrivals of approximately 7,000 seismic events recorded by Spanish (IGN) and Moroccan (CNRST) seismic networks. Both bulletins have been individually and jointly processed using the double-difference algorithm (*HypoDD*) and a regionally optimized velocity model. This approach significantly improved hypocentral precision, reducing event scatter and delineating a clearly defined, near-vertical seismic conduit-oriented NW–SE. Spatiotemporal analyses revealed distinct episodes of seismic migration, consistent with episodic fluid overpressure pulses, confirmed by diffusivity values (1.2–13.9 m²/s) characteristic of fluid-controlled swarms. Focal mechanisms predominantly indicated strike-slip motion, aligning with the regional transtensional tectonics and pinpointing the unrecognized Ras Tarf Fault as the primary seismogenic structure likely linked to the Al-Idrissi Fault System (AIFS). Integration with vertical and horizontal shear-wave velocity models (VSH and VSV) highlighted velocity anomalies at depths of 30–70 km, suggesting the presence of partially serpentinized mantle wedges above a delaminating slab segment, further supporting fluid involvement. Our results emphasize the critical interplay between deep lithospheric fluids, inherited fault structures, and regional tectonic stress, providing a comprehensive framework for understanding the 2021-2022 swarm dynamics which could improve the seismic hazard assessment in the region.

1. Introduction

Seismic swarms, characterized by clusters of earthquakes occurring without a dominant mainshock, are widely observed in both tectonic and volcanic settings (Danre et al., 2021; Ide, 2001; Ross et al., 2020). Unlike classical mainshock–aftershock sequences, swarms often exhibit complex spatiotemporal behaviors driven by transient stress changes, fluid migration, or aseismic slip (De Barros et al., 2019; Hainzl, 2004; Shelly et al., 2013; Sibson, 1996). High-pressure fluid interactions with fault zones are increasingly recognized as fundamental triggers of swarm-like seismicity (Cox, 2016; Shelly et al., 2013). Observational and modelling studies show that fluid intrusions can locally reduce fault strength and initiate swarms, while evolving stress redistribution sustains their progression (Hainzl, 2004). Recent numerical simulations further reveal that pulses of over-pressured fluids migrating upward can dynamically alter fault behaviour (Zhu et al., 2020), offering new insights into how energy is released and fault systems evolve over time.

The 2021–2022 seismic swarm in the Southern Alboran Sea stands out as one of the most exceptional and long-lasting seismic crises in the westernmost Mediterranean. Over a period of +700 days, the swarm produced more than 6,000 events (Mw > 1.5) (www.ign.es), concentrated offshore near the Moroccan coast of Al Hoceima. Although this study analyzes a 700-day window, seismic activity has persisted beyond this period, indicating the swarm ongoing. Seismic activity in the Al Hoceima region is

https://doi.org/10.5194/egusphere-2025-6433
Preprint. Discussion started: 21 April 2026

typically characterized by moderate-magnitude, (Bezzeghoud and Buforn, 1999; Grevemeyer et al., 2015), with no prior record of such prolonged or complex swarms, highlighting the exceptional nature of this sequence. In recent decades, the region has experienced significant seismic events such as the 1994 Mw 6.0 and 2004 Mw 6.4 Al Hoceima earthquakes, as well as the 2016 Mw 6.5 Alboran Sea event (Biggs et al., 2006; Buforn et al., 2017; Kariche et al., 2018; Tahayt et al., 2009). These past major events were marked by classical mainshock–aftershock sequences, in contrast to the 2021–2022 swarm, which lacked a clear mainshock and exhibited prolonged, migrating seismicity. More recent efforts have begun to explicitly address and characterize this type of prolonged seismic activity in Alboran region (Bouhali et al., 2025; Lozano et al., 2025).

The tectonic evolution of the Alboran region is shaped by a set of competing geodynamic mechanisms that have been proposed to explain present-day deformation. These include: (1) back-arc extension driven by the westward rollback of an eastward-subducting slab driven by the collision of the Nubia against Iberia (e.g. Faccenna et al., 2004; Lonergan and White, 1997); (2) slab break-off (e.g. Blanco and Spakman, 1993); (3) crustal extrusion across the Eurasia–Africa plate boundary (e.g. Rebaï et al., 1992); and (4) delamination and convective removal of the lithospheric mantle root (e.g. Calvert et al., 2000; Seber et al., 1996). Geodetic observations (e.g. Fadil et al., 2006) suggest a model supporting the active rollback and delamination of a subcontinental lithospheric slab beneath the Rif Mountains. Tomography models show crustal thinning, mantle flow reorganization, and asthenospheric upwelling (Arroucau et al., 2021; Bezada et al., 2013; Palomeras et al., 2014). The deep-seated processes, involving mantle flow and crustal thinning, are thought to facilitate partial melting and fluid migration from the upper mantle into the lower crust (Cavalcante et al., 2016; Plimmer, 2025). The resulting fluid or melt-rich zones may alter the thermal and mechanical properties of fault systems, influence stress conditions (Díaz-Alvarado et al., 2024) and promoting fault reactivation in the upper crust.

In this work, we investigate the link between the 2021–2022 Alboran Sea swarm and the active mantle dynamics in a tectonically complex domain. This study integrates and harmonizes earthquake bulletins from both the Moroccan National Centre for Scientific and Technical Research (CNRST) and the Spanish Instituto Geográfico Nacional (IGN), creating a unified, high-resolution dataset of P and S arrivals picks. Addressing the limitations of prior studies, we apply the *hypoDD* double-difference relocation algorithm (Waldhauser, 2001; Waldhauser and Ellsworth, 2000) using a regional seven-layer 1D velocity model derived from tomography studies including Morocco and Spain (Arroucau et al., 2021). This model offers improved consistency over the distinct velocity models previously used by the two agencies. The relocation procedure employs optimized clustering, damping, and iterative reweighting strategies to achieve high-precision hypocentral solutions. Thus, we integrate and relocate the combined earthquake catalogues using this unified velocity model to reduce inconsistencies and improve spatial resolution. This methodological advancement enables more accurate identification of active tectonic features and potential seismic hazards. We then analyze the swarm migration patterns and calculate diffusivity to test whether its evolution is consistent with a fluid-driven process, as suggested by recent modelling efforts for similar contexts. By addressing this question, we aim to advance the understanding of interactions among crustal structure, fluid migration, and fault reactivation in complex tectonic environments. Furthermore, our findings contribute to seismic hazard assessment methodologies and offer valuable insights for future investigations of swarm seismicity in comparable geodynamic settings.

2. Seismotectonic context

Geologically, the Alboran domain developed during Neogene times as a back-arc basin behind the retreating Tethyan slab, comprising metamorphic basement, Miocene to Quaternary sedimentary basins, and volcanic features such as the Alboran Ridge and Maimonides Seamount (Lonergan and White, 1997; Platt et al., 2013). These volcanic complexes reflect episodic mantle upwelling and decompressional melting during lithospheric thinning and rifting (Saunders et al., 2007). Moreover, seafloor structures such as mud volcanoes, sedimentary diapirs, and hydrothermal vents point to recent over-pressured fluid systems which can further influence fault slip and earthquake generation (Giammanco et al., 2008; Orange et al., 1999). The

https://doi.org/10.5194/egusphere-2025-6433
Preprint. Discussion started: 21 April 2026

region is marked by a network of active fault systems (Fig. 1), most prominently the Al-Idrissi Fault Zone (AIFZ), a NE–SW trending dextral strike-slip fault exhibiting transtensional kinematics and acting as a major locus of strain release during recent earthquakes (Galindo-Zaldivar et al., 2018; Lafosse et al., 2020). Complementary fault structures of the Trans-Alboran Shear Zone (TASZ), and the Nekor Fault extend this deformation field, linking offshore seismicity with onshore deformation (Buforn et al., 1995; Galindo-Zaldívar et al., 2015; Negredo et al., 2002). These fault systems are clearly imaged in high-resolution multichannel seismic reflection data and bathymetric profiles (d'Acremont et al., 2014; Martínez-García et al., 2013), showing complex segmentation, vertical fault geometries, and connections to deeper crustal or mantle structures. Structural studies also suggest the existence of crustal-scale detachments or inherited zones of weakness, which focus strain and facilitate earthquake nucleation, particularly in the presence of fluids or melt (Custódio et al., 2016; Díaz-Alvarado et al., 2024).

The southern margin of Alboran Sea near Al Hoceima represents a critical sector of the western Mediterranean tectonic system, lying within a diffuse and complex boundary zone between the African and Eurasian plates. Present-day convergence across this region occurs at a rate of approximately 4–5 mm/yr in a NW–SE to NNW–SSE direction, but unlike typical plate boundaries, the deformation is distributed across a wide corridor encompassing the Betic-Rif orogen, rather than being accommodated by a single fault zone (Koulali et al., 2011; Platt et al., 2013; Tahayt et al., 2008). This broad deformation zone hosts an intricate interaction of tectonic processes including lithospheric delamination, slab rollback, and asthenospheric upwelling (Baratin et al., 2016; Civiero et al., 2020; Fadil et al., 2006; Palano et al., 2013), creating a highly dynamic crust–

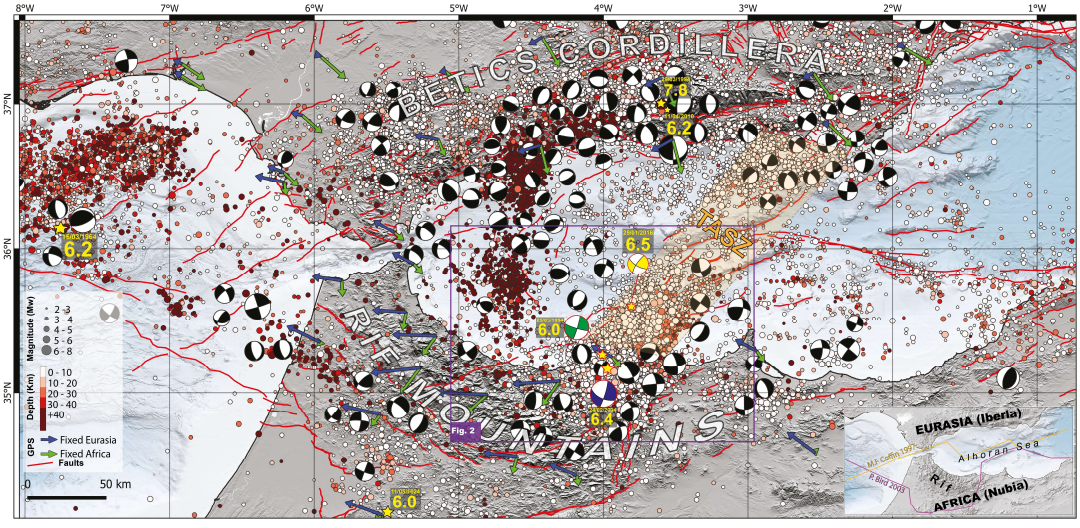

Figure 1: Seismotectonic framework of the Alboran region, northern Morocco, and southern Spain. The seismicity from the IGN Spain catalogue (1300–2024, M >2.5, coloured by depth), with major historical and instrumental earthquakes highlighted by yellow stars. Focal mechanisms of significant events (1990–2018) are shown (Buforn et al., 2017; Custódio et al., 2016; Martín et al., 2015). GPS velocity vectors (fixed Eurasia dark blue and fixed Africa green arrows, from Koulali et al., (2011). Faults (red lines) are from Zelenin et al., (2022). Bathymetry from EMODnet Digital Bathymetry (https://emodnet.ec.europa.eu/en/bathymetry - DTM 2022), and Digital Elevation Model is derived from Sentinel-1 images (using ESA - SNAP). TASZ: Trans-Alboran Shear Zone. The inset map represents the Eurasia-Nubia plate boundary across the Alboran.

mantle coupling that contributes to the regional seismicity. The rollback of the subducted slab beneath the Gibraltar Arc and its lateral tearing have been implicated in south-westward crustal block extrusion, as confirmed by GPS velocity fields and block kinematic models showing relative displacement and clockwise rotation of the Rif-Betic domain (Palomeras et al., 2017; Serpelloni et al., 2007; Tahayt et al., 2008a). These motions are associated with transtensional tectonics, as revealed by InSAR analyses of the Al Hoceima region, which indicate crustal deformation distributed across conjugate fault systems, both offshore and onshore (Akoglu et al., 2006; Galindo-Zaldívar et al., 2015; Tahayt et al., 2009).

Seismic tomography and ambient noise imaging further delineate the lithospheric architecture of the region, with high-velocity anomalies in the upper mantle interpreted as remnants of a subducted slab and low-velocity zones suggesting the presence of

https://doi.org/10.5194/egusphere-2025-6433
Preprint. Discussion started: 21 April 2026

fluids or partial melt in the crust and mantle wedge (Arroucau et al., 2021; Bezada et al., 2013; El Moudnib et al., 2015). These low-velocity domains may facilitate swarm-like seismicity by lowering effective normal stresses and enhancing pore pressure diffusion within fault zones (Hauksson and Unruh, 2007). Crustal structure models, including those by El Moudnib et al. (2015) and Palomeras et al. (2017), show strong lateral heterogeneities and thinning of the crust to less than 20 km beneath parts of the basin, confirming its back-arc extensional origin. Furthermore, numerical-modelling results offshore Southwest Iberia indicate ongoing delamination of old oceanic lithosphere along a serpentinized decoupling horizon, a mechanism that may facilitate subduction initiation and has been invoked to explain the region's largest historical earthquakes, including the 1755 Lisbon (M8.5–8.7) and 1969 San Vicente (M7.9) events (Duarte et al., 2025).

The Alboran domain exhibits dense, spatially heterogeneous seismicity (Fig. 1) driven by Nubia–Eurasia interaction (Buforn et al., 2011; Stich et al., 2010), with hypocenters from near-surface to >150 km depth (IGN; USGS) and a deep arcuate cluster from the Gulf of Ceuta toward the Granada zone that reaches ~600 km depth, consistent with a subducted slab beneath the Gibraltar Arc (Bezzeghoud and Buforn, 1999; de Lis Mancilla et al., 2018; Spakman and Wortel, 2004; Villaseñor et al., 2015). In the central basin, seismicity organizes within the NE–SW TASZ, where most events occur at 5–25 km depth (occasionally ~70 km depth) (Gràcia et al., 2012, 2019; Grevemeyer et al., 2015; Lafosse et al., 2020; Martínez-García et al., 2013; Medina and Cherkaoui, 2017; Perea et al., 2012). Magnitudes are dominated by Mw 2.5–4.0, punctuated by large shocks of 26 May 1994 Mw 6.0 (~13 km depth), 24 Feb 2004 Mw 6.4 (~9 km depth), 11 Apr 2010 Mw 6.3 (~650 km depth), and 25 Jan 2016 Mw 6.5 (~12 km depth), that together frame the region hazard (Akoglu et al., 2006; Bezada and Humphreys, 2012; Buforn et al., 2017; Cakir et al., 2006; Stich et al., 2020; Tahayt et al., 2009).

Epicentres cluster along the northern Moroccan margin in step with active structures, the Al-Idrissi, Trougout, Bokkoya, and Nekor fault systems offshore/onshore, and along structurally aligned belts in the Rif (Galindo-Zaldivar et al., 2018; Gràcia et al., 2019; Grevemeyer et al., 2015; Olaiz et al., 2025; Sanz de Galdeano et al., 2019; Somoza et al., 2021). Within this corridor, the Al Hoceima sector is the western Mediterranean most active area (Fig. 1) with Mw 4.0–5.0 events and occasional Mw ≥ 6 shocks recurring on decadal (~10–12 yr) timescales (Kariche et al., 2018; Tachema et al., 2023); depths there are largely 5–25 km, locally ~40 km offshore E–SE of the city. Focal mechanisms across the region are predominantly strike-slip with minor normal components (Fig. 1), consistent with a transtensional regime in which sinistral NE–SW systems (e.g., Al-Idrissi, Trougout and Bokkoya Faults) interact with dextral NW–SE faults (e.g. Yusuf Fault) (d'Acremont et al., 2020; Galindo-Zaldivar et al., 2019; Medialdea et al., 2004; Palano et al., 2013; Tendero-Salmerón et al., 2022). Geodetic and geologic constraints indicate ~1–3 mm/yr slip on major faults such as the Al-Idrissi and Nekor faults, with strain partitioned among multiple blocks and structures (Koulali et al., 2011; Poujol et al., 2014; Tahayt et al., 2008; Vernant et al., 2010). Given comparatively short fault lengths, the region's seismic moment release is high (Medina and Cherkaoui, 2017), a pattern attributed in part to episodic swarms and fluid-assisted rupture clustered along inherited structures, bathymetric highs, and crustal fluid zones (Kariche et al., 2018; Lozano et al., 2025).

The 1994 Mw 6.0 (~13 km depth) event ruptured Bousekkour-Aghbal strike-slip fault offshore Al Hoceima (e.g., El Alami et al., 1998; Bezzeghoud and Buforn, 1999); the 2004 Mw 6.3 shock (~9 km depth) nucleated near the Bokkoya strike-slip system (e.g., Akoglu et al., 2006; Buforn et al., 2017; Tahayt et al., 2009); and the 2016 Mw 6.5 mainshock (~12 km depth) and its aftershocks aligned along the offshore continuation of the Al-Idrissi Fault Zone, delineating steep, NE–SW segments with activity focused at 5–25 km depth (Buforn et al., 2017; Galindo-Zaldivar et al., 2018; Grevemeyer et al., 2015; Lozano et al., 2025; Medina and Cherkaoui, 2017; Stich et al., 2005, 2020) (Fig. 2a).

The most recent crisis, the 2021–2022 Alboran swarm, occurs as an unusual and long-lived seismic episode within this highly active sector. Hypocentres from the Moroccan CNRST and Spanish IGN datasets delineate a ~30 km-thick, NW–SE-trending

https://doi.org/10.5194/egusphere-2025-6433
Preprint. Discussion started: 21 April 2026

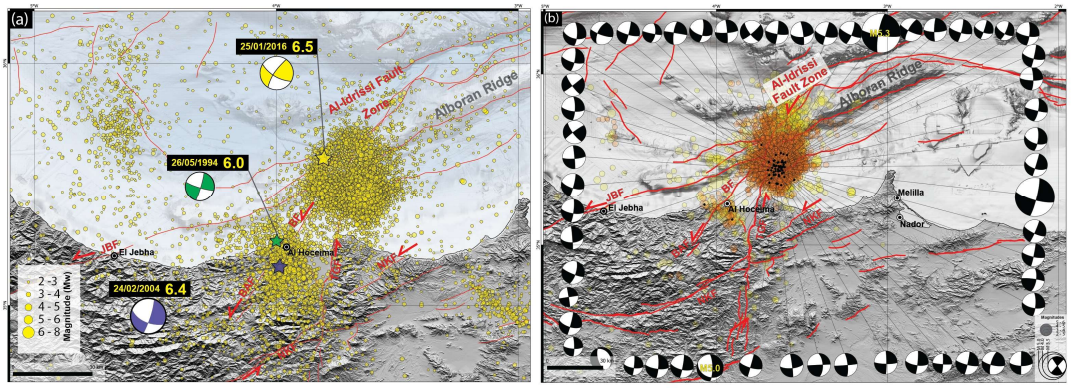

Figure 2: (a) Displays the complete seismic catalogue from 1300 to 2024 (M>2), compiled from the Spanish IGN catalogue, highlighting the long-term seismic activity of the region, major historical earthquakes (1994, 2004, and 2016) (Kariche et al., 2018). (b) shows the seismicity between 01/01/2021 – 01/01/2023 from Moroccan (CNRST yellow-coloured) and Spanish (IGN orange-coloured), along with focal mechanism solutions from (www.ign.es). Active fault structures mapped in red in both maps are the Al-Idrissi Fault Zone, JB: Jebha Fault, NKF: Nekor Fault, TGF: Trougout Fault, BF: Bokkoya Fault, BAF: Bousekkour-Aghbal Fault. Bathymetry and Digital Elevation Model are the same as in Figure 1.

seismic column positioned between the southern termination of the Al-Idrissi Fault and the northern tip of the Trougout Fault (Fig. 2b). The swarm generated numerous moderate-magnitude earthquakes (Mw 4.0–5.3) but lacked a clear mainshock, in sharp contrast to earlier sequences dominated by a single large event. Instead, it unfolded as a protracted, episodic sequence, potentially driven by mixed processes. The 2021–2022 seismic swarm lies in a complex context, of a crustal manifestation of deeper lithospheric and mantle dynamics including slab rollback, crustal extension, and fluid migration. Understanding this system requires the integration of high-resolution relocation methods with improved velocity models (Arroucau et al., 2021; Lozano et al., 2025) on a catalogue merging from both sides of the Alboran Sea.

3. Data and methods

The earthquake bulletins used in this study are provided by the Moroccan National Center for Scientific and Technical Research (CNRST) and the Spanish National Geographic Institute (IGN). These datasets consist of P- and S-wave arrival times recorded by seismic stations around the region affected by the 2021–2022 seismic swarm, bounded between 34.70°N and 36.20°N latitude and 5.10°W to 2.95°W longitude (Fig. 3a). The analyzed events range in magnitude from 1.5 - 5.7 Mw and depths between 0 - 110 km. The swarm persisted for over 700 days. The IGN catalogue spans the full period from January 3, 2021, to January 1, 2023, while the CNRST catalogue covers the interval from June 25, 2021, to December 29, 2022. A comparison of event counts shows that the IGN catalogue includes 3,720 events, while the CNRST catalogue contains 3,483 events. Combined, these datasets provide more than 135,000 arrival-time picks. The IGN catalogue includes 43,126 P-wave and 45,723 S-wave picks, totalling 88,849 travel-time differences across 32 seismic stations. The CNRST catalogue contributes 27,313 P-wave and 21,256 S-wave picks, totalling 48,569 travel-time differences from 17 stations. These discrepancies reflect variations in network coverage, detection thresholds, and temporal completeness. To address these differences and enhance spatial resolution, the datasets were integrated and jointly analyzed, providing a more robust constraint on the structure and dynamics of the seismic swarm.

The decision to merge the CNRST and IGN catalogues is scientifically critical given the location of the 2021–2022 Alboran swarm at the boundary between the Moroccan and Spanish seismic networks (Fig. 3a), where neither network alone provides optimal azimuthal coverage. Earthquake location accuracy is strongly dependent on the geometric distribution of stations relative to the seismic source; poor azimuthal coverage can lead to biased hypocentral depths, increased lateral scatter, and uncertainties in fault-plane geometry (Bondár et al., 2004; Husen and Smith, 2004). In border regions between networks,

https://doi.org/10.5194/egusphere-2025-6433
Preprint. Discussion started: 21 April 2026

single-network solutions often suffer from limited station density on one side of the source, causing asymmetric error ellipses and artificial elongation of seismicity patterns (Schaff and Richards, 2004). By combining arrival-time picks from both Moroccan and Spanish stations, the merged dataset significantly improves azimuthal coverage, increases the number of P- and S-wave observations per event, and enhances depth resolution. This integrated approach has been successfully applied in previous cross-border studies of seismic sequences (e.g., Schaff and Waldhauser, 2005), demonstrating that catalogue merging reduces systematic biases, improves spatial clustering, and better constrains rupture geometries. In the context of the Alboran swarm, such methodological integration is indispensable for accurately resolving its spatiotemporal evolution and for providing robust constraints on the seismotectonic processes operating in this complex plate boundary zone.

To merge the catalogues, events were matched based on exact timestamps including date, hour, and minute, but excluding seconds and fractional seconds. Only events with identical origin times in both catalogues were retained, yielding a merged dataset of 5,330 events. For these common events, P- and S-wave picks from both Moroccan and Spanish stations were combined, which improved azimuthal coverage and increased the average number of picks per event to 8. To ensure the quality of the phase data, only events assigned quality classes A, B, or C from *Hypo71* (Lee and Lahr J.C, 1972) were retained.

Initial earthquake locations were computed using the *HypoInverse* algorithm (Klein, 1989) over 15 iterations, applying a consistent 1D velocity model from Arroucau et al., (2021) across all stations, without applying station corrections. This model provides a regionally optimized representation of seismic velocity structure, offering an improvement over the ak135 global model (Kennett & Engdahl, 1991) used in the original CNRST catalogue and the customized velocity model employed by IGN (Tab. 1), a fixed Vp/Vs ratio of 1.73 was used (Fig. 3b). The initial *HypoInverse* solutions yielded very low RMS residuals, ranging from 0.00 to 0.30 seconds, indicating an excellent match between observed and theoretical arrival times.

The relocated hypocentres were then refined using the double-difference algorithm implemented in *HypoDD* (version 2.1b) (Waldhauser and Ellsworth, 2000), which minimizes the residuals between observed and predicted travel-time differences between pairs of nearby events. The relocation used only catalogue-derived differential times, as no waveform cross-correlation data were available. The ph2dt utility was used to convert phase arrivals into the differential-time format required

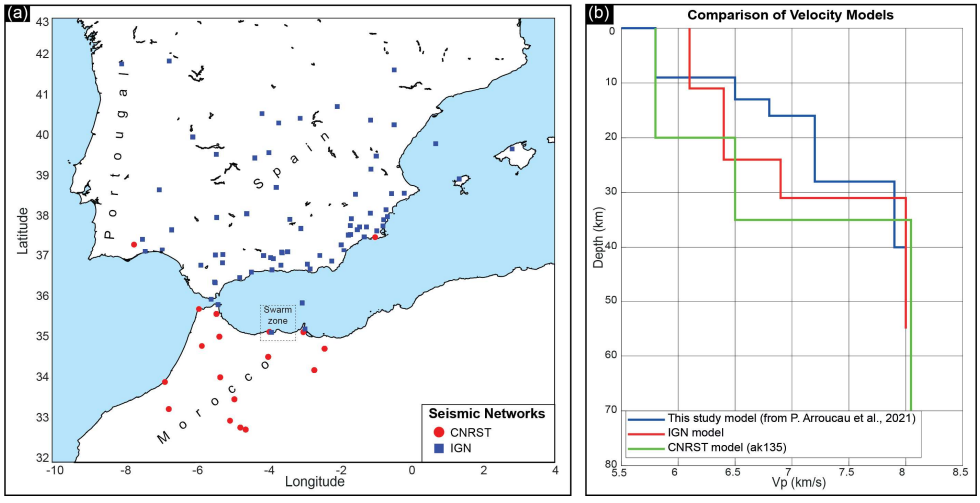

Figure 3: Seismic networks and velocity models and used in this study. (a) Seismic networks map of CNRST (Morocco) red and IGN (Spain) blue respectively and marks the region of interest (2021–2022 swarm). (b) Comparison of velocity models (P-wave) used for earthquake relocation.

Table 1: Comparison of layered P-wave velocity (Vp) models for the Western Alboran region, showing depth interfaces and corresponding velocities for the models used in this study (Arroucau et al., 2021), the IGN model, and the CNRST-ak135 model.

Arroucau et al., 2021	IGN Spain	CNRST Morocco (ak135)

https://doi.org/10.5194/egusphere-2025-6433
Preprint. Discussion started: 21 April 2026

Depth (km)	Vp (km/s)	Depth (km)	Vp (km/s)	Depth (km)	Vp (km/s)
0	5.5	0	6.1	0	5.8
9	5.8	11	6.1	20	6.5
13	6.5	24	6.4	35	8.4
16	6.8	31	6.9	77.5	8.045
28	7.2	55	8	120	8.050
40	7.9	-	-	-	-
55	8	-	-	-	-

by *HypoDD*. The process was conducted using configuration parameters consistent with those previously applied to the individual CNRST and IGN catalogues to ensure methodological consistency. Events were linked in clusters with a maximum separation of 5 km and a maximum event-to-station distance of 400 km. Each event was connected to a minimum of five and a maximum of ten neighbours to ensure a robust linkage network. The relocation was conducted over six iterations, and weighting factors were adjusted dynamically throughout the process. The catalogue differential travel-time weight was typically set between 5 and 10, and the damping factor was fixed at 20 to stabilize the inversion. This iterative reweighting strategy led to a more coherent spatial distribution of events.

After merging, a total of 3,525 events were successfully relocated. Events with both high horizontal and vertical (>10 km) uncertainties were excluded, while those with acceptable errors in at least one dimension were retained (<10 km horizontal and/or <10 km vertical errors). The results revealed significant lateral and vertical adjustments in hypocentre locations. Compared to the initial *HypoInverse* solutions, the relocated events displayed improved spatial clustering and confinement. These changes were particularly notable when comparing the merged relocations with the CNRST-only catalogue, which showed considerable scatter. In contrast, differences between the merged and IGN-only solutions were smaller due to the higher initial station density and better azimuthal coverage of the IGN network (Fig. 3a). The final RMS residuals for the *HypoDD* solutions (RCT values) ranged from 0.0 to 1.2 seconds, with a median of 0.38 seconds for the three catalogues. Although higher than the *HypoInverse* values (0.25) due to the use of catalogue differential times, these results still indicate a reliable and consistent improvement in hypocentral resolution.

4. Results

4.1 Relocation analysis

The relocated hypocentres of the 2021–2022 swarm from the Spanish IGN and Moroccan CNRST catalogues demonstrate significant improvements in location accuracy, particularly in terms of spatial clustering and depth resolution (Fig. 4). The analysis compares initial and relocated seismicity, revealing substantial differences in swarm extent and structure, both horizontally and vertically. For the IGN catalogue, 3,666 events were initially available, of which 1,820 were successfully relocated. The CNRST catalogue contained 3,459 events, with 2,124 successfully relocated. In both cases, the relocation process refined the spatial distribution of events, reduced scatter, and concentrated seismicity within more distinct seismogenic zones, reflecting improved hypocentral precision (Fig. 4a and b). These enhancements are primarily attributed to the use of a regionally optimized velocity model and the application of the double-difference relocation technique (*HypoDD*). In addition to the separate catalogue relocations, a combined dataset was constructed by matching common events between IGN and CNRST catalogues based on exact origin times. This merged catalogue included 5,330 events, from which 3,525 were successfully relocated using joint phase data from both national networks (Fig. 4c). The integration of seismic picks from both Moroccan and Spanish stations significantly improved azimuthal coverage and increased the number of arrivals per event, leading to further refinement in hypocentre locations (Tab. 2). The combined relocation results show even tighter clustering

https://doi.org/10.5194/egusphere-2025-6433
Preprint. Discussion started: 21 April 2026

of events and enhanced depth resolution, highlighting the benefits of cross-network data fusion in resolving complex swarm structures (Fig. 4c).

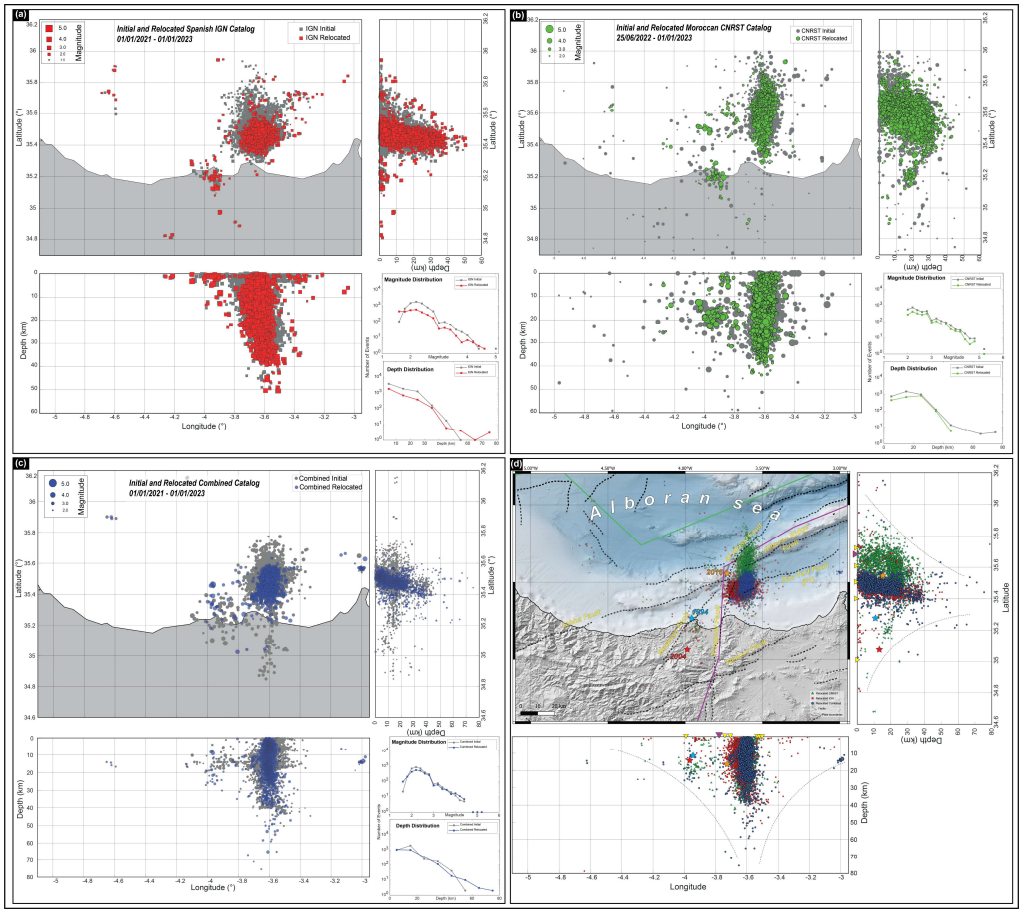

Figure 4: Comparison of initial and relocated earthquake catalogues for the 2021–2022 South Alboran swarm from the IGN (a), CNRST (b), combined (c). Map views display the distribution of seismicity, with initial locations (grey) and relocated positions red squares (IGN), green circles (CNRST), and blue circles (combined) catalogues. Inset bottom right corner curves in (a), (b), and (c) summarize statistical variations in the number of events by magnitude and depth before (grey) and after (coloured) relocation. (d) Map of the South Alboran region displaying relocated seismicity from all datasets. Active fault (black dashed), yellow triangles indicate the intersection of fault onto the vertical cross-sections. Significant earthquakes are marked with coloured stars in d: blue (1994 Mw 6.0), red (2004 Mw 6.4), and orange (2016 Mw 6.5) (Kariche et al., 2018). Purple and green lines correspond to plate boundaries from Bird (2003) and Coffin et al. (1998), respectively.

4.1.1 Spatial Distribution and Seismicity Patterns

The 2021–2022 Alboran seismic swarm relocation, from the Spanish IGN and Moroccan CNRST catalogues demonstrate substantial improvements in location accuracy, with tighter spatial clustering and sharper depth resolution. In Figure 4, the grey dots correspond to initial locations obtained with *HypoInverse*, whereas the coloured dots represent refined *HypoDD* locations, highlighting the increased coherence of the seismicity after relocation. The map-view and the cross-sections reveal differences in geometric distribution between the two catalogues: the relocated IGN events form a nearly circular cluster suggesting a compact rupture zone, while the CNRST events display a more elongated, north-south pattern, possibly reflecting broader deformation coverage or limitations due to network configuration (Fig. 4a and b).

The relocation of the combined catalogue further enhanced hypocentral resolution by leveraging seismic picks from both national networks. As shown in (Fig. 4c), the relocation results yield a dense, well-clustered distribution of events, especially

https://doi.org/10.5194/egusphere-2025-6433
Preprint. Discussion started: 21 April 2026

in map view, highlighting the benefit of cross-network integration. The initial locations (grey dots) are more scattered, especially at the swarm's periphery, while the relocated events (blue dots) concentrate along a narrow, spheroid trend oriented approximately NW–SE, reflecting the likely orientation of the active fault zone (Fig. 4d).

In cross-section view (Fig. 4c) along longitude vs. depth, the relocated events delineate a near-vertical structure that narrows at depth and extends to nearly 70 km. This configuration contrasts with the initial locations, which show greater vertical scatter. The latitude–depth cross-section shows that relocated events form a focused south-dipping structure, consistent with regional faulting, and the side-by-side of mechanically contrasting units (soft Alboran Basin sedimentary infill and (Ras Tarf and BAIV volcanic rocks). The improved depth clustering further confirms the enhanced accuracy gained through joint relocation. In support of this, the magnitude and depth distribution plots in Fig. 4c reveal that while the magnitude-frequency content remains consistent pre- and post-relocation, the depth histogram shows a tighter concentration of events in the 10–40 km depth range after relocation. This reduction in vertical scatter illustrates the role of improved network geometry in constraining hypocentral depth. Together, these findings emphasize how network configuration affects location geometry, and demonstrate that merging catalogues under a unified relocation scheme not only improves event resolution but also reduces bias introduced by individual network limitations.

4.1.2 Statistical Analysis

The statistical curves (Fig. 4) provide a comparison between the initial and relocated catalogues, offering insights into depth distribution and magnitude-frequency trends. The magnitude-frequency distribution follows a typical trend, with the majority of earthquakes occurring within the 2.5–3.5 magnitude range. This distribution is consistent across both catalogues, indicating that the relocation process does not significantly alter the magnitude characteristics of the swarms. However, the depth distribution for both Moroccan and Spanish catalogues reveals that most events are concentrated at shallow to intermediate depths, displaying a clearer peak at depths of 15–25 km (Fig. 4a and b). This reinforces the improvement in depth constraints achieved through the relocation process. In addition to the individual national catalogues, the merged relocation results further confirm these trends. Thus, the magnitude distribution remains consistent after relocation, but the depth curves reveal a more focused concentration of events between 15–20 km, with reduced vertical scatter compared to the initial merged catalogue (Fig. 4c).

Relocation performance differs across catalogues but improves the geometric coherence of the swarm. From the initial event sets (CNRST = 3,483; IGN = 3,720; merged = 5,330), *HypoInverse* locates 99.3% of CNRST (3,459/3,483), 98.5% of IGN (3,666/3,720), and 99.2% of the merged set (5,285/5,330). *HypoDD* then relocates 2,124 CNRST events (61.0% of initial; 61.4% of *HypoInverse*), 1,820 IGN events (48.9% of initial; 49.7% of *HypoInverse*), and 3,525 merged events (66.2% of initial; 66.7% of *HypoInverse*), i.e., the merged catalogue yields both the largest relocated population and the highest relocation fraction. *HypoInverse* median RMS lies between 0.18–0.25 s (CNRST = 0.20, IGN = 0.18, merged = 0.25), whereas the *HypoDD* residual RMS is 0.36–0.39 s (CNRST = 0.36, IGN = 0.39, merged = 0.38); because these metrics are computed on different datasets (absolute vs. differential times), their absolute values are not directly comparable and the *HypoDD* RMS should not be interpreted as a deterioration of fit. Reported 1-σ location uncertainties are 4.1/2.1/2.5 km for *HypoInverse* (CNRST/IGN/merged) and 7.80/9.71/7.95 km for *HypoDD*. This pattern is expected: the double-difference solution optimizes relative geometry within clusters (evidenced by tighter spatial patterns in Figs. 2), while absolute uncertainties remain controlled by the poor station geometry in the offshore swarm area (no stations directly north of the swarm and the nearest stations located several tens of kilometres away), as well as by inter-network heterogeneity and pair connectivity (Husen and Hardebeck, 2010; Waldhauser, 2001; Waldhauser and Ellsworth, 2000; Zhang and Thurber, 2003). Notably, the merged catalogue's broader station coverage and higher event-pair linkage produce the largest, most coherent relocated cluster despite somewhat larger absolute σ than the single-network *HypoInverse* baselines.

https://doi.org/10.5194/egusphere-2025-6433
Preprint. Discussion started: 21 April 2026

4.2 Spatiotemporal analysis

4.2.1 Spatiotemporal and Migration Maps

The spatiotemporal evolution of the 2021–2022 seismic swarm in the southern Alboran Sea, as resolved in the relocated CNRST, IGN, and combined catalogues reveals a progressive spatial contraction of seismicity, both horizontally and vertically, over the course of the sequence (Fig. 5). In the early stages, particularly during mid-2021, seismicity was more dispersed, extending laterally over several kilometres and vertically to depths exceeding 40 km. However, as the swarm advanced, earthquakes became increasingly confined within a narrower and more coherent rupture zone, indicating a self-organizing process characteristic of swarm-type sequences.

In the CNRST relocation (Fig. 5a), early activity (Jun–Aug 2021) is diffuse over ~35.30–35.90° N and −3.80 to −3.40° E, spanning ~0–45 km depth. Through late 2021 the cloud collapses into a narrow north–south corridor linking onshore Al Hoceima to the offshore network. By mid- to late-2022, the swarm is tightly concentrated near 35.53–35.57°N, −3.62 to −3.56°E, with a core plan-view width of ~5–7 km that flares asymmetrically to the north and east (a halo extending ~8–12 km). Hypocenters are dominantly ~8–30 km deep, with few outliers deeper than ~35 km. Cross-sections indicate a near-vertical column that shows a modest southward deepening in latitude–depth (dip ~60°) and a steeper, almost vertical profile in longitude–depth (≥75–85°) consistent with activation of a steep, N–S-to-NNE-SSW segment of the local faults relay. The column is slightly wider to the north and east, where shallow (<10–12 km) and intermediate-depth events form a sparse apron

https://doi.org/10.5194/egusphere-2025-6433
Preprint. Discussion started: 21 April 2026

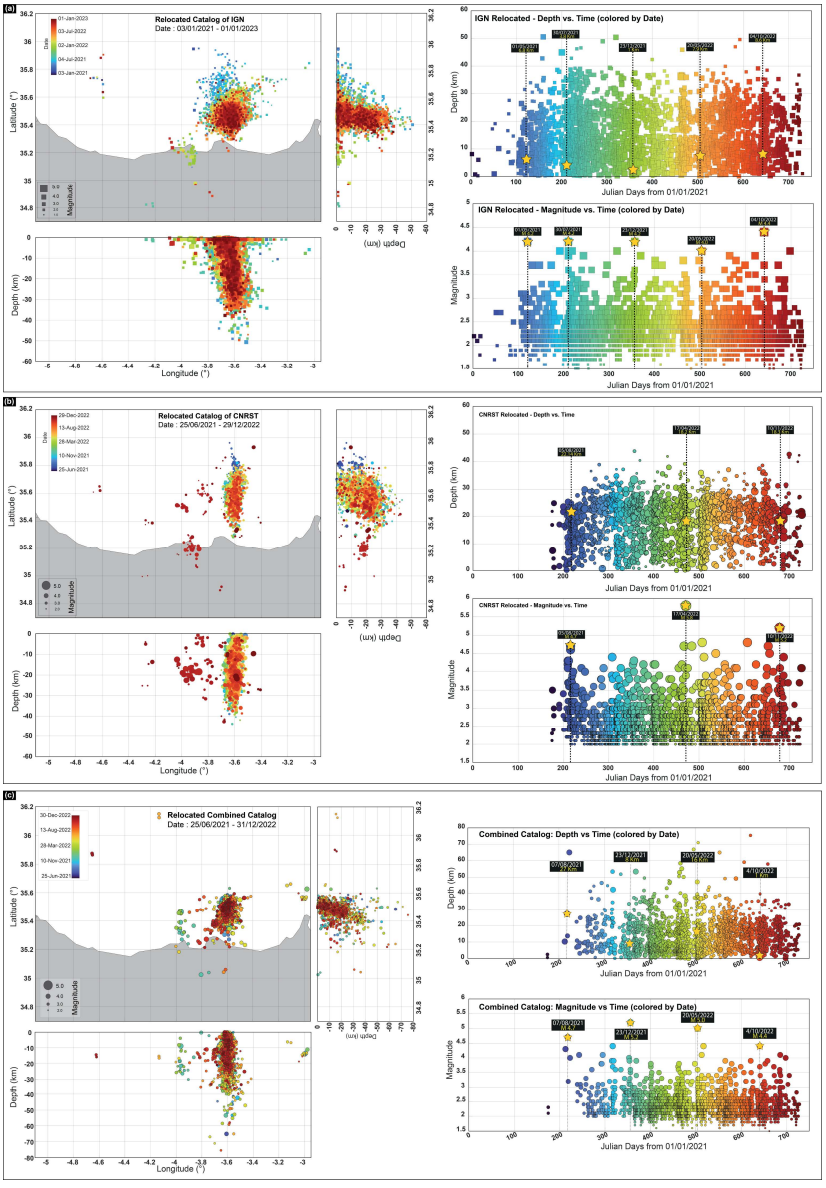

Figure 5: Spatiotemporal evolution map and cross-sectional views of the 2021–2022 seismic swarm in the IGN (a), CNRST (b), and Combined (c) relocated catalogues. Yellow stars indicate large-magnitude events (+M4).

https://doi.org/10.5194/egusphere-2025-6433
Preprint. Discussion started: 21 April 2026

Table 2. Event counts and quality metrics for the 2021–2022 South Alboran swarm. For CNRST, IGN, and the merged catalogue, we report initial events, located solutions (*HypoInverse*), relocated solutions (*HypoDD*), and the median travel-time RMS (s) and median Horizonal uncertainty (km).

	CNRST	IGN	Merged
Initial number of events	3483	3720	5330
Number of located events (*Hypoinverse*)	3459	3666	5285
Number of relocated events (*HypoDD*)	2124	1820	3525
Hypoinverse RMS	0.2	0.18	0.25
***Hypoinverse* location uncertainty (km)**	**4.1**	**2.1**	**2.5**
HypoDD RMS	0.36	0.39	0.38
***HypoDD* location uncertainty (km)**	**7.80**	**9.71**	**7.95**

around the core. Temporally, the tightening is punctuated by moderate events (e.g., M 4.7 on 5 Sep 2021, M 4.6 on 10 Nov 2022), but the sequence remains mainshock-less, with moment release distributed over episodic bursts rather than a single through-going rupture.

On the other hand, the IGN catalogue, benefiting from station density and broader temporal coverage (03/01/2021 – 01/01/2023), provides a higher-resolution image of the swarm's development (Fig. 5b). Initially, seismicity commenced in the northern part of the region, close to the rupture zone of the 2016 Mw 6.5 Alboran earthquake. Throughout 2021, events extended from near-surface levels to depths approaching 50 km, gradually migrating southeast ward toward the onshore (Ras Tarf volcanic massif) (Fig. 5b). By late 2022, seismic activity concentrated within a narrow vertical corridor at depths between 10 and 20 km. Map-view analysis highlights a clear transition from an initially diffuse seismic cloud to a well-defined NW–SE-aligned rupture zone, indicative of focused fault reactivation and/or structural border. Cross-section profiles further illustrate this progression, revealing a steeply dipping fault-aligned structure extending downward to approximately 70 km, with a pronounced southward dip of (≈70º) evident in latitude–depth sections.

In the IGN relocation (Fig. 5b), the longer window (03 Jan 2021–01 Jan 2023) resolves a two-phase spatial evolution. Early 2021 earthquakes form a diffuse cluster north of the main zone at roughly 35.60–35.80° N, -3.65 to -3.50°, spanning ~0–50+ km depth. Through mid-2021 the activity shifts ~10–20 km to the southeast, concentrating near 35.53–35.58° N, -3.62 to −3.56° and reducing its plan-view footprint from ~10–12 km to ~4–6 km. By late 2022, hypocenters are tightly clustered in a near-vertical corridor with a modal depth band of ~10–20 km, deep outliers to ~35–55 km are largely confined to 2021. Cross-sections show an apparent southward dip of ~65–75° in latitude–depth across 10–30 km, and a near-vertical (≥80–85°) profile in longitude–depth. The column is asymmetrically wider to the north and east by ~2–4 km relative to the southwest flank. Depth- and magnitude-versus-time panels document episodic bursts (e.g., 01-May 2021, 30-Jul 2021, 23-Dec 2021, 20-May 2022, 04-Oct 2022) with short-lived depth excursions; the magnitude ceiling remains ~4.5–4.8, and no single event dominates the sequence. Overall, the IGN record captures a north to southeast migration and progressive focusing into a narrow, steep column that stabilizes at ~10–20 km depth by the end of 2022. Altogether, the IGN view reinforces a mainshock-less, columnar swarm that narrows through time, dips slightly south in section, and widens asymmetrically to the southeast, consistent with reactivation of a steep AIFZ–Ras Tarf segment at the edge of the BAIV structural high.

Enhanced azimuthal coverage and increased numbers of phases per event resulted in tightly clustered hypocenters and significantly reduced depth uncertainties, confirming a coherent, NNW–SSE to NW–SE-trending seismogenic structure consistent with previously identified tectonic features (AIFZ and Trougout faults), but rather linked to a new reactivated segment. From a temporal-spatial perspective, the combined catalogue highlights a three-stage migration pattern. The first stage (mid to late 2021) shows deepening seismicity, with events progressively reaching depths of ~35–40 km, culminating in a moderate M4.7 earthquake on 7 August 2021. The second stage, spanning early to mid-2022, starts with the M5.2 on 23

https://doi.org/10.5194/egusphere-2025-6433
Preprint. Discussion started: 21 April 2026

December 2021, marks an upward migration and an extensive activity and densification of events between 15 and 25 km depth, the end of this stage coinciding with the M5.0 shock on 20 May 2022. The third stage, extending through late 2022, features a highly localized and vertically confined cluster (its depth major reached ≈20 km), peaking with another burst including an M4.4 on 4 October 2022. The early scattered seismicity followed by spatial tightening over time reflects a likely interplay between regional tectonic stress accumulation and localized fluid migration. The later-stages, however, could indicate a reactivation of a narrow rupture zone, with increasing structural control and possible weakening due to stress buildup.

The combined relocated catalogue (Fig. 5c), integrating picks from both Moroccan and Spanish networks, offers the most comprehensive and consistent image of the swarm geometry, and spatiotemporal behaviour. The enhanced azimuthal coverage breakdowns the scattered cloud into a compact column at 35.53–35.58° N, −3.62 to −3.56° E, (i.e., at the junction of the southern AIFZ, Trougout, and the inferred Ras Tarf (F1) segment) and immediately north of the BAIV high. Plan-view width of the core cluster is ~5–7 km, with a sparse peripheral scatter extending ~8–12 km to the north and east. Cross-sections show a near-vertical to steep structure: in latitude–depth the column exhibits an apparent southward dip of ~65–75° through the 10–30 km band; in longitude–depth it is ≥80–85°. Depth distribution tightens from an early envelope of ~5–60+ km to a modal band of ~10–20 km by late 2022, with the deepest outliers confined to the first months of the sequence. Time plots resolve three phases without invoking mechanism: (i) Mid–late 2021, progressive deepening with scattered events to ~35–40 km, including M 4.7 on 07 Aug 2021; (ii) Late 2021–mid 2022, upward focusing and densification within ~15–25 km, spanning the M 5.2 on 23 Dec 2021 and M 5.0 on 20 May 2022; (iii) Late 2022, a highly localized, vertically confined cluster with most events ~10–20 km, culminating in a burst including M 4.4 on 04 Oct 2022. Overall, the merged view documents a north to southeast consolidation into a steep, NNE–SSW/NE–SW–aligned corridor co-located with the AIFZ–Trougout–F1 junction at the flank of BAIV, with asymmetric widening toward the south and east and a stable magnitude ceiling below Mw ~5.0.

4.2.2 Depth-time and Magnitude-time plots

The depth–time and magnitude–time panels (Fig. 5) resolve how the 2021–2022 sequence evolved in size and depth. After HypoDD relocation, events cluster into discrete time windows separated by quieter intervals, and spurious surface fixes (0 km) are removed and repositioned at mid-crustal depths. Importantly, the depth plots confirm this correction, which is most pronounced during the second and third stages of the swarm, underscoring the relocation's ability to recover the genuine cyclic pattern. The cyclic bursts are clearly visible and are typically initiated by a moderate event (e.g., Mw 4.7 (07 Aug 2021), Mw 5.2 (23 Dec 2021), Mw 5.0 (20 May 2022), Mw 4.4 (04 Oct 2022)) followed by cascading sequences of smaller earthquakes. As the sequence progresses, magnitudes remain dominated by Mw ~2.0–3.5, while the active depth band narrows from an early broad range (near surface to ~50–70 km) to recurrent mid-crustal depths of ~10–20 km.

Catalogue by catalogue, the temporal character is consistent with variant resolutions. In IGN (03/01/2021–01/01/2023), relocation separates previously overlapping clusters: larger events occur at the onset of burst episodes and are followed by dense sequences of smaller magnitudes, with active-window depths mostly ~10–25 km and the deepest outliers confined to early 2021. CNRST (25/06/2021–29/12/2022) shows the same episodic structure at lower resolution: post-relocation, cluster onsets/terminations are clearer and the larger events repeatedly occur at depth ~15–25 km. The combined catalogue (25/06/2021–31/12/2022) provides the clearest chronology: (i) mid–late 2021 progressive deepening with events to ~35–40 km (e.g., Mw 4.7 on 07 Aug 2021); (ii) late 2021–mid 2022 upward focusing with sustained activity at ~15–25 km (spanning Mw 5.2 on 23 Dec 2021 and Mw 5.0 on 20 May 2022); (iii) late 2022 recurrent clusters in the ~10–20 km band (e.g., Mw 4.4 on 04 Oct 2022). Across all three catalogues, larger-magnitude events tend to occur at the onset of bursts, followed by aftershock-like sequences, reinforcing the episodic nature of the swarm. In the combined catalogue these bursts are more clearly delineated, with greater separation between active and quiescent periods; this periodicity points to recurring stress perturbations or pressure transients, plausibly linked to slow fluid diffusion or stepwise fault activation (e.g., Cattania and Segall, 2021; Hainzl, 2004; Parotidis and Shapiro, 2004; Shapiro and Dinske, 2009; Vidale and Shearer, 2006). The largest

https://doi.org/10.5194/egusphere-2025-6433
Preprint. Discussion started: 21 April 2026

events act as temporal anchors that mark transitions between stages, organizing the intervening smaller-magnitude activity. Although a few key shocks in the single-network catalogues could not be relocated (insufficient event–pair links for stable differential-time inversion), the merged catalogue compensates by improving temporal coverage and recovering a more complete burst structure.

Taken together, the stable magnitude ceiling (≤ Mw ~5) and the persistent mid- to upper-crustal depths (~10–25 km) indicate reactivation of a pre-existing, steep strike-slip structure rather than progressive loading toward a larger mainshock. In the context established earlier, the active depth range matches the expected seismogenic levels of the Al-Idrissi–Trougout–Ras Tarf system at the flank of BAIV. The short inter-burst intervals (months) likely limited stress accumulation, so moderate events were followed by swarms of small earthquakes without escalation. A slow-slip/creep component on parts of the network (consistent with low continuous slip rates along Bokkoya; Vidil et al., 2025) and transient fluids as a modulating, but not sole, agent together provide a coherent explanation for the observed timing and depth ranges. Thus, the burst sequence is best viewed as the temporal expression of ongoing transtensional reactivation on existing AIFZ–Trougout–Ras Tarf segments within the BAIV-bounded corridor, and is far from implying the development of a new structure.

4.3 Fluid Diffusivity and Time Distance (RT plot) analysis

To investigate the migration behaviour of the 2021–2022 seismic swarm, we analyzed the spatiotemporal evolution of relocated earthquakes along several key cross sections. For each section, we computed the distance of individual hypocentres from the initial event and plotted this distance as a function of event origin time. These radius-time (RT) plots provide a robust framework to identify and quantify potential diffusion-like migration patterns. In multiple cases, the outer bounds of the seismicity displayed a parabolic shape consistent with pore-pressure diffusion models. To assess this quantitatively, we compared the observed migration patterns with theoretical diffusion envelopes derived from Shapiro et al., (1997), expressed in Eq. (1), where “r” is the distance from the source, “t” is the elapsed time, and “D” is the hydraulic diffusivity.

$$r = \sqrt{4\pi D t}\ , \tag{1}$$

The time–distance (RT) analysis of the 2021–2022 seismic swarm offers critical insights into the spatiotemporal migration behaviour of seismicity in the western Alboran Sea (Fig. 6, 7 and, 8). Using the relocated catalogues from the Spanish IGN, Moroccan CNRST, and the merged dataset, we observe consistent patterns of swarm propagation characterized by radial expansion from the initial hypocentre, with varying degrees of spatial clustering and events diffusivity. This pattern is typically attributed to fluid-driven or stress-triggered migration processes acting on pre-existing crustal faults. Before describing the migration patterns of the 2021–2022 swarm, it is important to distinguish between phases that follow a Mainshock–Aftershock (MS–AS) sequence and those that initiate without a dominant mainshock. In MS–AS phases, seismicity starts with a relatively large event (M ≥ 4) followed by a rapid succession of smaller earthquakes, whereas non–MS–AS phases display a more progressive onset and lack a clearly defined mainshock. This distinction is essential because high apparent migration velocities in MS–AS sequences can arise not only from fluid-related processes but also from dynamic stress transfer triggered by the mainshock (e.g., Harris, 1998; Hill et al., 1993; Parsons, 2002). In the 2021–2022 Alboran swarm, early January 2021 (IGN catalogue) and December 2021 (merged catalogue) represent MS–AS-type bursts, while several mid-2022 episodes are non–MS–AS, exhibiting migration patterns more typical of swarm-like activity.

In the IGN catalogue (Fig. 6), the initial RT diagram reveals a progressive radial expansion of seismicity from the onset in early January 2021, reaching distances of up to ~45 km by early 2023. The corresponding fluid diffusivity values range from 1.2 to 13.9 m²/s, with several burst-like sequences aligning along diffusivity theoretical curves. After relocation, the IGN dataset (Fig. 6b) shows a more coherent propagation of seismicity, with sharper clustering of events, particularly within the D = 3.5 to 8.1 m²/s envelopes. Larger-magnitude events (M > 4.0), such as those in April and July 2021, tend to initiate or coincide with the start of each swarm burst, indicating possible fluid overpressure or slip-induced triggering. Thus, explaining

https://doi.org/10.5194/egusphere-2025-6433
Preprint. Discussion started: 21 April 2026

the absence of larger earthquakes (M = 6) in the sequence. These moderate events could act as stress-release valves (Nakajima and Hasegawa, 2021; Oth, 2013; Zhou et al., 2025), periodically relieving accumulated strain on localized fault patches. By preventing prolonged stress buildup, they might inhibit the conditions necessary for larger ruptures. Finally, the improvement in depth constraints also reduces near-surface artifacts and clarifies the migration trend, further supporting fluid involvement at mid-crustal levels.

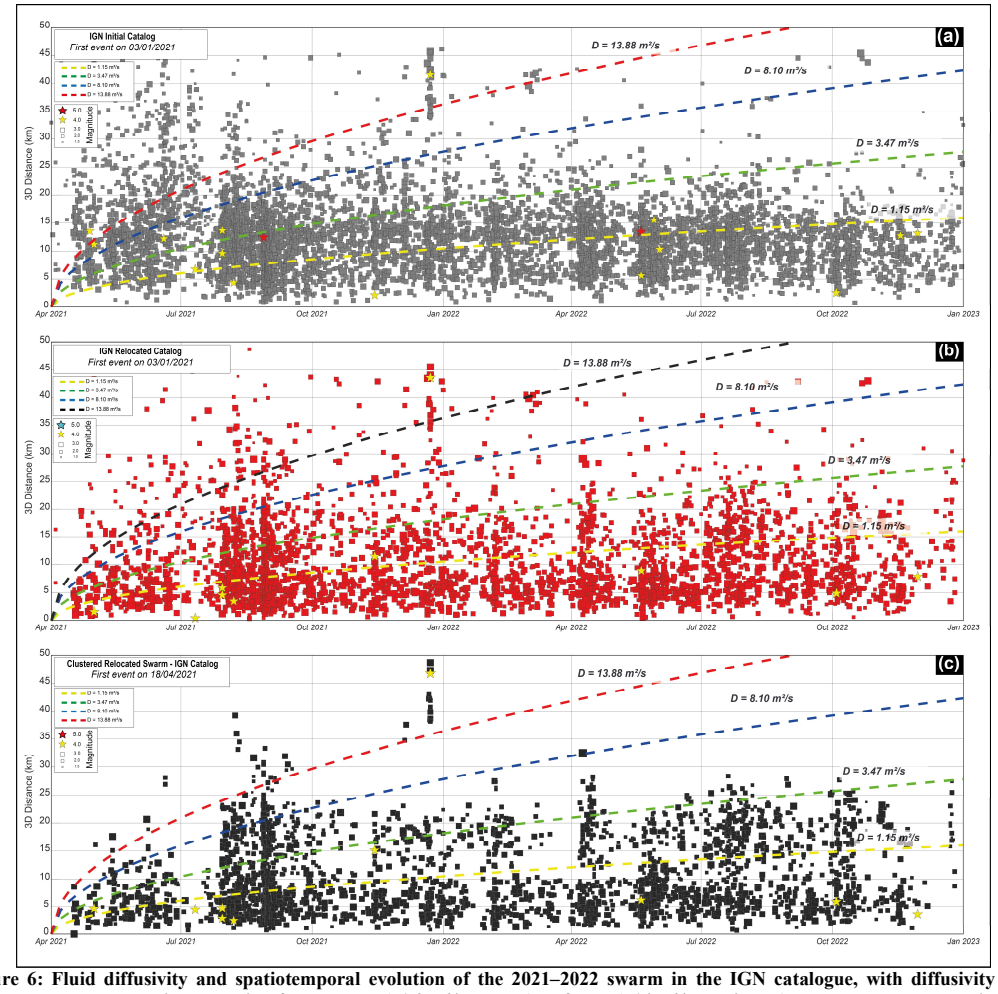

Figure 6: Fluid diffusivity and spatiotemporal evolution of the 2021–2022 swarm in the IGN catalogue, with diffusivity rates represented by dashed lines, ranging from slower (~1.2 m²/s, yellow) to faster (~14 m²/s, red/black). Yellow and red stars indicate events with magnitudes ≥M4 and ≥M5, respectively. Panel (a) initial, (b) relocated, and (c) clustered relocated events identified using the Reasenberg clustering function in Zmap https://github.com/swiss-seismological-service/zmap7 (Wiemer, 2001).

The CNRST catalogue (Fig. 7), with its initial event recorded on 25 June 2021, exhibits a more scattered migration signature in its original version. Seismicity spreads radially up to ~40 km, but with greater dispersion and less distinct clustering. The diffusivity ranges remain consistent (1.2 to 13.9 m²/s), but fewer events fall within the defined envelopes, suggesting limitations due to lower station coverage (Fig. 7a). The relocated version, however (Fig. 7b), reveals clearer propagation features and burst segmentation. Several early bursts in mid to late 2021 align with the D = 3.5–8.1 m²/s envelopes, though the scatter remains higher than in the IGN dataset. This again reflects the impact of station density on relocation precision. Despite this, the largest CNRST events (e.g., M4.7 in September 2021) are temporally aligned with other bursts seen in IGN, confirming that both catalogues capture the same broad migration episodes with varying resolution.

https://doi.org/10.5194/egusphere-2025-6433
Preprint. Discussion started: 21 April 2026

The most refined and physically coherent representation of swarm migration emerges from the combined catalogue (Fig. 8). The initial catalogue displays similar scatter to the single-network versions (Fig. 8b), but after relocation, the migration becomes significantly clearer, with burst episodes sharply defined in time and space. The clustered version of the combined RT plot (Fig. 8c) reveals five major seismic bursts propagating outward from the origin point with velocities ranging from 1.5 to 4.5 km/day, consistent with moderate to high diffusivity levels observed in fluid-driven swarms elsewhere. Similar rates occur in the Westmorland, California swarm (1–3 km/day; Lengliné et al., (2017); CO_2-driven), the Vogtland NW Bohemia region (2-5 km/day; Hainzl et al., (2012); deep CO_2), and Iceland's Hengill system (0.5–4 km/day; Jousset et al., (2011); hydrothermal fluids). These parallels strengthen the case for fluid overpressure as the primary driver of fault slip in our study. These bursts are distinctly segmented, with each one showing a fast acceleration phase followed by a slowdown, suggesting discrete fluid pulses and/or episodes of stress release. Each burst in the combined catalogue (occurring around August 2021, December 2021, March 2022, July 2022, and October 2022) matches both the occurrence of moderate to large events (e.g., M5.2 on 23 December 2021, M5.0 on 20 May 2022) and the onset of newly activated seismic patches in the map and cross-section views. Their alignment with calculated RT envelopes further supports a diffusion-like migration pattern, with D values predominantly between 1.15 and 8.10 m^2/s. Notably, the highest velocity burst (~4.5 km/day) corresponds to the third phase, initiated just before the M5.2 event, and is followed by a sudden contraction in event distribution, likely indicating a release of overpressure or exhaustion of available pathways for fluid migration. In this case, the rapid migration could also reflect possible dynamic stress transfer, whereas smaller-magnitude bursts within the swarm are more plausibly controlled by fluid migration processes. Taken together, the combined catalogue RT plot confirms that the 2021–2022 seismic swarm evolved as a series of fluid-assisted migration episodes.

The episodic expansion of hypocentres in space and time, their correspondence with moderate-magnitude triggering events, and their alignment with theoretical diffusivity trends are all consistent with the behaviour of fluid-influenced swarms observed in volcanic, geothermal, and tectonic settings globally. Moreover, the progressive reduction in burst extent toward the final months of 2022 reflects a waning of the swarm-driving mechanism, potentially due to decreasing fluid availability or the stabilization of critically stressed fault patches. The integration of IGN and CNRST datasets in a unified catalogue proves essential for fully resolving the swarm dynamics. It reduces localization uncertainty, enables consistent burst identification, and highlights indirect differences between phases. The high fidelity of the clustered RT plot underscores the value of joint relocation and catalogue harmonization for seismic swarm studies, especially in border-complex regions where cross-network collaboration enhances scientific resolution. Ultimately, this detailed RT analysis validates the interpretation that fluid migration, likely from lower crustal or upper mantle sources, played a central role in modulating the timing, migration rate, and structure activation patterns of the 2021–2022 South Alboran seismic swarm.

https://doi.org/10.5194/egusphere-2025-6433
Preprint. Discussion started: 21 April 2026

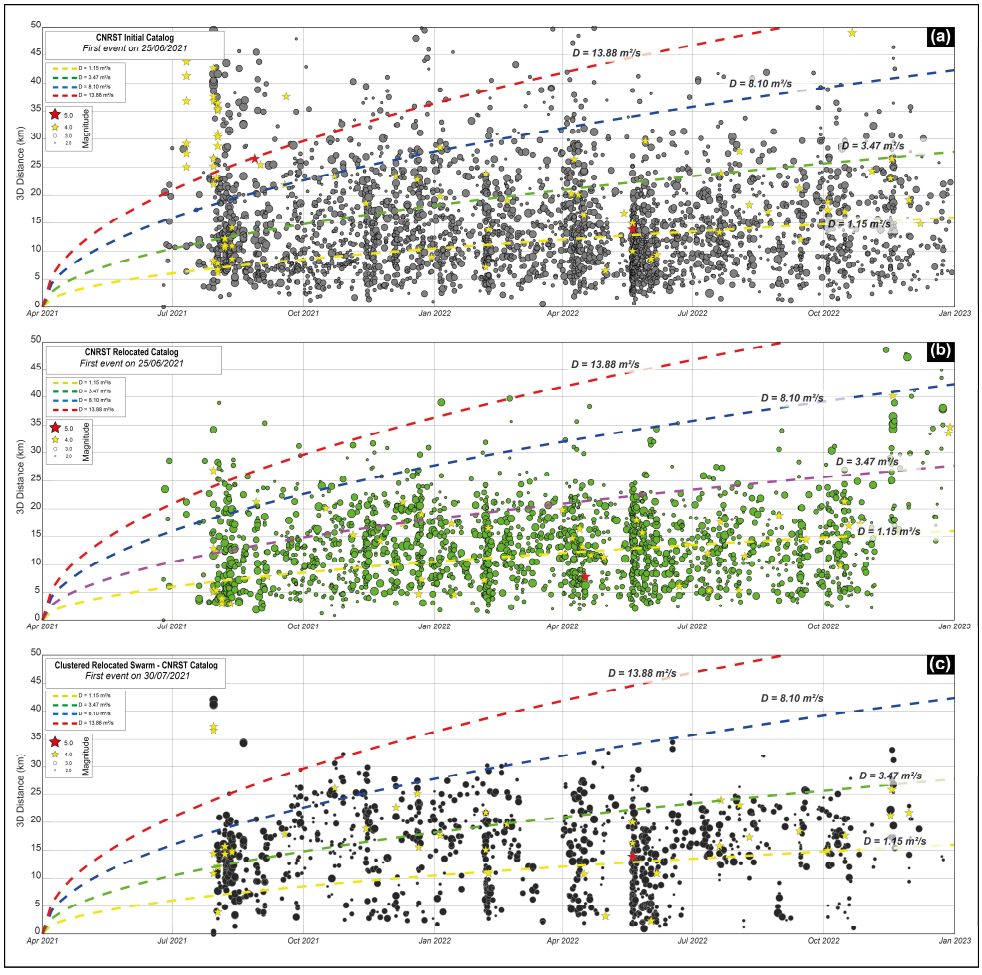

Figure 7: Same as Figure 6 for the CNRST catalogue.

4.4 The 2021 – 2022 Swarm focal mechanisms

The regional stress field is oblique to the major structures, with ENE–WSW shortening and NNW–SSE extension, so slip is partitioned onto conjugate strike-slip sets as suggested for the 2004 Al Hoceima fault (Tahayt et al., 2009). Sinistral motion concentrates on NE–SW to NNE–SSW strands (AIFZ and Ras Tarf), while dextral motion is taken up by NW–SE faults that bound the Trans-Alboran Shear Zone. In this configuration, the structural node where the southern Al-Idrissi Fault Zone intersects the western Alboran Ridge and links toward the Trougout trend focuses shear, induces local stress rotations, and promotes releasing bends and step-overs (e.g. Galindo-Zaldivar et al., 2018; Gràcia et al., 2019; Lafosse et al., 2020; Poujol et al., 2014; Soumaya et al., 2018; Stich et al., 2020; Tendero-Salmerón et al., 2021). These geometric elements predict small normal components superimposed on dominantly strike-slip kinematics, and they provide natural pathways for along-strike propagation (Fig. 9).

The 2021–2022 swarm matches these expectations (Fig. 9a–b): Epicenters define a narrow NE–SW corridor centred on the southwest offshore tip of Ras Tarf Fault, bracketed by the southern AIFZ, the northern Trougout and Bokkoya faults. Depth sections show a steep, near-vertical to moderately dipping seismogenic surface from approximately 2 to 18–20 km depth, with two density bands at about 3–8 km and 10–18 km. Focal mechanisms from the IGN catalogue cluster in the strike-slip domain with minor normal components (Fig. 9c), and nodal planes are sub-parallel to Ras Tarf fault (NE–SW) and to the AIFZ (NNE–

https://doi.org/10.5194/egusphere-2025-6433
Preprint. Discussion started: 21 April 2026

SSW). The two largest events, Mw 5.1 on 28 August 2021 and Mw 5.3 on 20 May 2022, share this geometry and occur on the same NE–SW system, indicating moment release on inherited, high-angle strike-slip segments rather than on newly formed planes. The tendency for shallower events to lie northeast of Ras Tarf fault and deeper events to step slightly southwest is consistent with along-strike propagation into adjacent segments at depth, where local releasing bends add the observed normal components.

The cluster overlies the Big Al-Idrissi Volcano (BAIV), a buried volcanic edifice whose summit coincides with the Messinian reflector imaged by seismic reflection profiles and that is onlapped by Pliocene–Quaternary strata (Lafosse et al., 2020; Vidil et al., 2025). BAIV constitutes a structural high, and the surrounding shelf experienced contrasting vertical motions through time: earlier uplift and outward building are recorded around the volcanic high, followed by shoreline backstepping and transgression beginning after about 1.81 Ma, which are attributed to tectonic subsidence linked to right-stepping N–S normal faults and AIFZ splays. Immediately to the southwest, the Bay of Al Hoceima shows a fault-bounded, bathymetric low that reflects ongoing subsidence, with a graben or half-graben geometry defined by the Bokkoya, Bousekkour-Aghbal fault array to the west and the Trougout, Boudinar and Ras Tarf faults system to the east (Fig. 9). This pairing of an elevated, fractured volcanic basement at BAIV and a subsiding trough in the bay creates strong lateral contrasts in rheology, permeability, and stress, which can focus shear and fluids along relay zones. Within this framework, it is plausible that BAIV acts as a lateral seismogenic boundary, a partial barrier to rupture and fluid diffusion, helping confine the swarm within the BAIV–Ras Tarf corridor while maintaining the dominantly strike-slip focal mechanisms imposed by the regional field.

Taken together, the focal mechanisms are the expected kinematic expression of the ongoing transtensional regime, the fault network behaves as a segmented, high-angle strike-slip system with local releasing bends, and the swarm records the translation of this regime into time-dependent seismic activity. The junction or relay architecture explains the tight lateral footprint and the substantial vertical extent, the slight southwest deepening is consistent with propagation into adjacent segments at depth, and transient fluid overpressure and stress transfer provide a plausible means for episodic growth and migration between the shallow and deep bands. The combined influence of inherited strike-slip fabrics, right-stepping N–S normal faults, and the BAIV volcanic basement, together with the subsiding Al Hoceima graben, defines a mechanically and hydraulically heterogeneous corridor that governs where seismicity could, and could not, propagate during the 2021–2022 sequence.

https://doi.org/10.5194/egusphere-2025-6433
Preprint. Discussion started: 21 April 2026

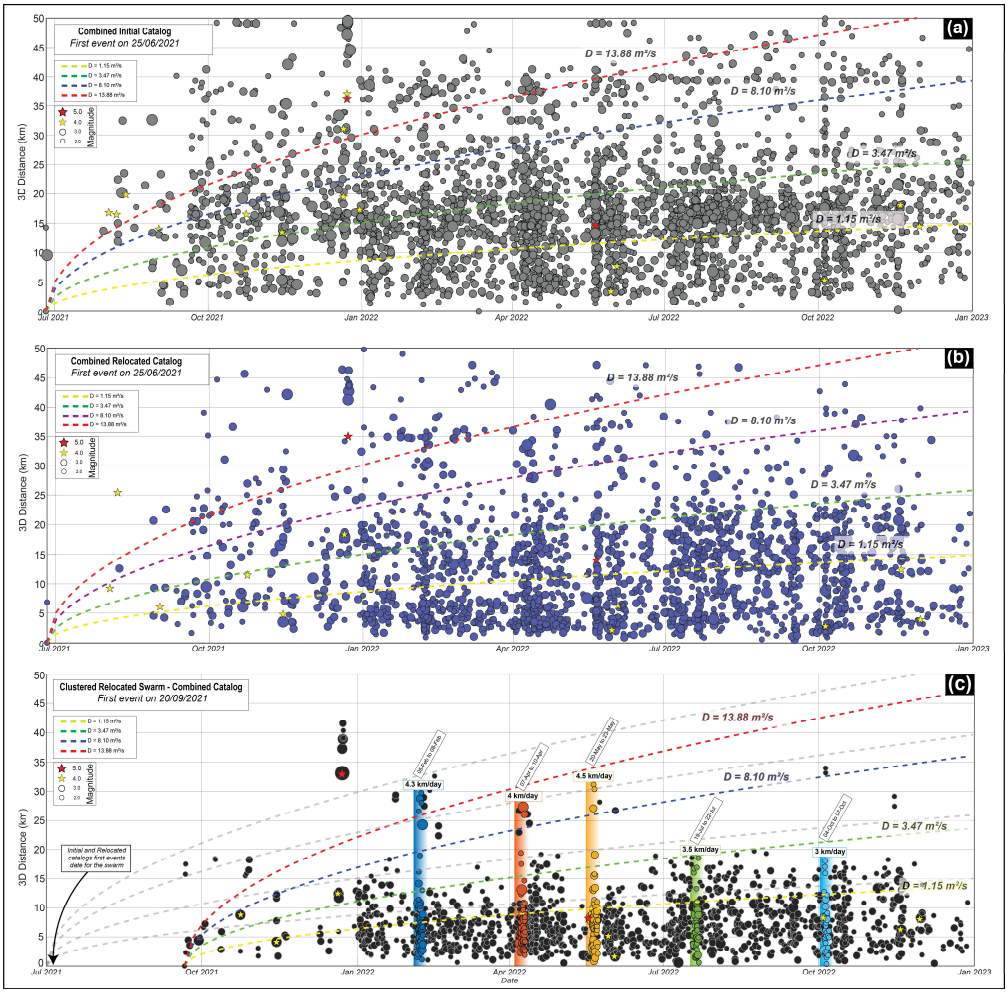

Figure 8: Same as Figure 6 for the combined catalogue (c), coloured events (dark blue, orange, yellow, green, and light blue) represent velocity bursts calculated over 3-day windows.

4.5. Crustal- lithospheric structure and its relationship with the 2021–2022 seismic swarm

The Collaborative Seismic Earth Model (CSEM) Iberia-2019 shear-wave fields (VSH, VSV) (Trabant et al., 2012) place the 2021–2022 swarm within a heterogeneous lithosphere that varies strongly across short lateral distances (Fig. 10). Depth slices and the two transects show a narrow NE–SW corridor where shear velocities are relatively low compared to the surrounding blocks. This corridor is co-linear with the TASZ including the Ras Tarf and the Al-Idrissi system. It overlies the BAIV structural high, and it is located north of the subsiding Al Hoceima Bay. The map panels also show that the TASZ and the Alboran Ridge coincide with, or sit immediately adjacent to, faster domains. Seismicity, including the 2021–2022 sequence, clusters along the margins of these faster regions, which highlights the importance of velocity gradients rather than any single endmember of the velocity field.

In the shallow crust (0–10 km), both VSH and VSV delineate a NE–SW low-velocity corridor of about 3.0–3.5 km s^{-1} beneath the central Alboran basin and offshore Rif. The combined relocated epicenters fall within this band, immediately northeast of Ras Tarf fault and near the mapped intersections among the TASZ, the Al-Idrissi and Yusuf faults, and the Ras Tarf Fault. Shallow low-V anomalies are widely interpreted as fractured, fluid-rich or thermally weakened rock (Gea et al., 2023; Hensen et al., 2019; Maestro-González et al., 2008; Maiorana et al., 2024; Porkoláb, 2021), so their coincidence with the swarm implies

https://doi.org/10.5194/egusphere-2025-6433
Preprint. Discussion started: 21 April 2026

reduced effective strength and elevated permeability where inherited strike-slip structures can be reactivated. The corridor narrows toward the Bokkoya–Ras Tarf–AIFZ junction, which suggests a focusing of weakness where fault relays have been mapped in marine geophysical surveys (d'Acremont et al., 2020; Lafosse et al., 2020). The mid-crust (10–20 km) retains the NE–SW alignment of the shallow band, although absolute speeds increase to roughly 3.8–4.2 km s^{-1}. A relatively low-V stripe persists beneath the swarm and tightens toward the Bokkoya–Ras Tarf–AIFZ junction in both VSH and VSV, consistent with a vertically connected weak zone. Such a zone could be a long-lived damage band within the strike-slip system or a set of mechanically weakened mafic intrusions that later became part of the fault network. Hypocenters extend through this depth range while maintaining the same plan-view trend, which fits an interpretation in which fluids and shear localize within the same mid-crustal corridor.

At lower-crustal depths (≈20–35/40 km), both sections reveal a faster "lid" beneath the central Alboran Basin (≈4.3–4.7 km s^{-1}) bordered by slower flanks. The steep velocity gradient along the edge of this lid coincides with the deepest part of the sequence where present (≈40–55 km), which indicates that stresses concentrate at the margins of a rigid block. This geometry is compatible with mafic underplating or reworked lower-crustal and lithospheric fragments associated with delamination and slab rollback (Calvert et al., 2000; Spakman and Wortel, 2004). The main mapped plate-boundary strands that cut the basin, including AIFZ and Yusuf, lie along or near the same gradients, which explains why deformation localizes there even though individual fault planes are below tomographic resolution. In the upper mantle (≈35–60 km depth), shear speeds generally exceed 4.5 km s^{-1}, with localized High-V pockets of roughly 4.8 km s^{-1} appear beneath Betics basin.

The deepest hypocenters fall at, or just outside, the edge of the lid of Hige-V at ~50 km depth. This pattern is consistent with a locally weakened mantle lid and/or a hydrated, thermally softened asthenosphere in a geodynamic setting influenced by the Gibraltar slab system (Gea et al., 2023). Modest thermal anomalies and/or limited partial melt would sharpen permeability and rheology contrasts, promoting focused upward fluid transfer and pressure transients that can feed mid- to upper-crustal fault networks, consistent with observations of focused fluid discharge in the West Alboran domain and with established fault-zone hydro-mechanical models (Blinova et al., 2011; Faulkner et al., 2010; Sibson, 1992). The fault network drawn in Fig. 10, which includes the AIFZ, the Alboran Ridge system, and Yusuf, lines up with the principal velocity contrasts rather than with uniform low-V domains. Faster, mechanically stronger blocks appear to concentrate stress, and strain is guided onto bordering

https://doi.org/10.5194/egusphere-2025-6433
Preprint. Discussion started: 21 April 2026

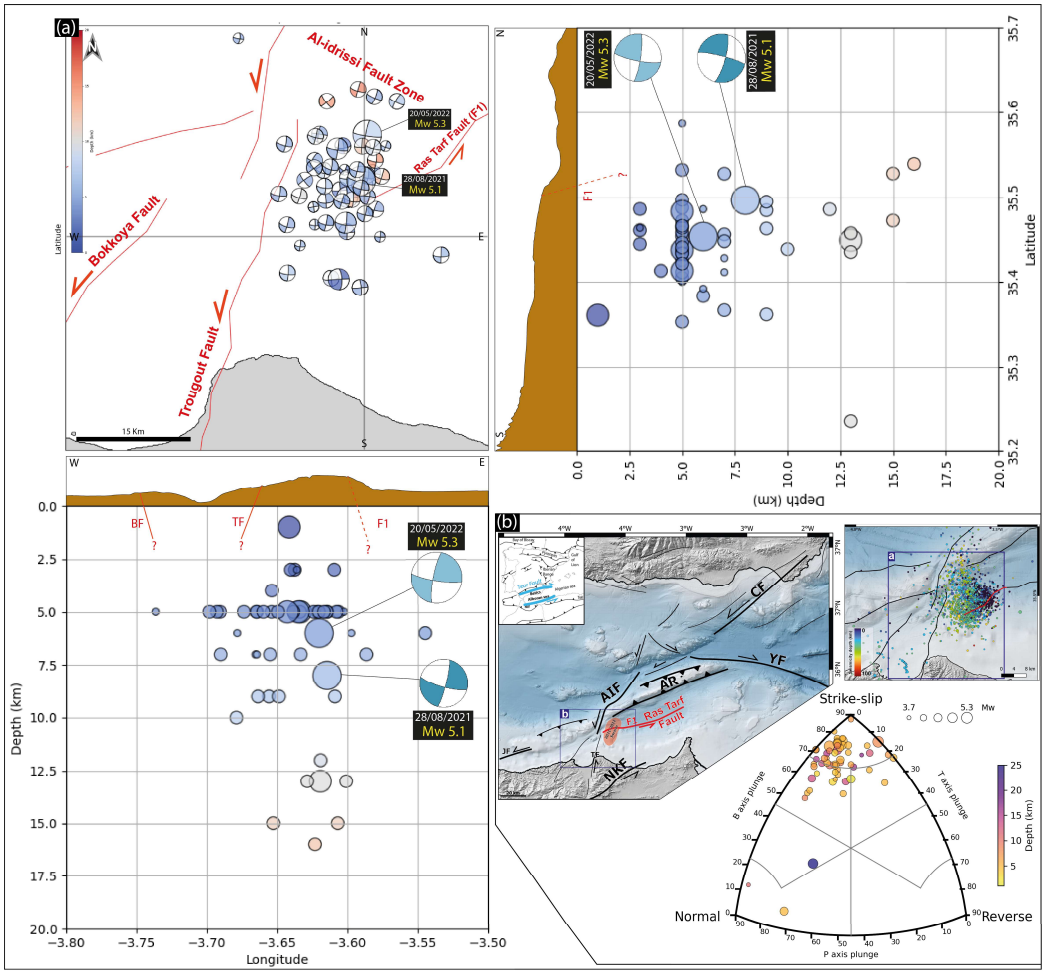

Figure 9: Alboran regional tectonic context and active faults in the region are Ras Tarf Fault (F1) outlined in red. (a) Map and (EW) and North-South (NS) cross-section views of distribution of focal mechanism solutions for the 2021–2022 swarm events, recorded between January 17, 2020, and January 7, 2023 (www.ign.es). (b) map of the seismicity of the 2021-2022 Alboran swarm relocated and combined catalogue. AIF: Al-Idrissi Fault; YF: Yusuf Fault; CF: Carboneras Fault; NKF: Nekor Fault; Jebha Fault; AR: Alboran Ridge; BF: Bokkoya Fault, TF: Trougout Fault. The ternary diagram provide classification of the 2021 – 2022 swarm events focal mechanisms, which predominantly exhibit a strike-slip faulting mode. Focal mechanism and ternary plots using FMC function by (Álvarez-Gómez, 2019).

faults that the tomographic model cannot resolve explicitly. The swarm's hypocenters and focal mechanisms described earlier are consistent with this picture: moment release occurs on steep, inherited strike-slip segments that are sub- parallel to faults (e.g., AIFZ), while small normal components appear where step-overs and segment tips create local releasing geometries.

A final observation from Fig. 10 concerns the relationship between absolute speeds and gradients. Many Alboran earthquakes, not only those in 2021–2022, occur close to the margins of higher-velocity domains tied to the Trans-Alboran and Alboran Ridge systems. The 2021–2022 sequence respects this rule: shallow and mid-crustal events occupy the low-V corridor immediately adjacent to faster lower-crustal structure, while the deepest events sit near the transition from slower to faster mantle. This pattern indicates that velocity contrasts, and the mechanical contrasts they imply, are key in determining where strain localizes and how swarms evolve. Taken together, the tomography and the seismicity support a coherent scenario. Regional transtension funnels shear onto NE–SW strike-slip segments, velocity gradients around strong blocks focus stresses onto their borders, and fluids (with possible minor magmatic inputs) exploit the same corridor to modulate effective strength and promote episodic failure (Calvert et al., 2000; Civiero et al., 2019; Gómez de la Peña et al., 2018; Palomeras et al., 2013;

https://doi.org/10.5194/egusphere-2025-6433
Preprint. Discussion started: 21 April 2026

Spakman and Wortel, 2004). The BAIV high and the fault-bounded Al Hoceima low provide the lateral framework that confines the sequence and explains its geometry. Although the CSEM is smoothed and cannot image individual faults, the match among velocity contrasts, mapped structures, plate-boundary models, and the 2021–2022 hypocentral distribution provides a process-based explanation for why the swarm arose and persisted in this part of the Alboran plate-boundary zone.

5. Discussion

This study presents a double-difference relocation of approximately 3,000 seismic events from the 2021–2022 seismic swarm in the southern Alboran Sea, offering new insights into the structural framework and underlying mechanisms driving seismicity in this tectonically complex region. We integrated phase data from both the Spanish IGN and Moroccan CNRST seismic networks and applied a consistent and optimized relocation workflow. Initial locations are obtained via *HypoInverse* followed by double-difference refinement using *HypoDD* in conjunction with a regionally appropriate 1D velocity model. We achieved significant improvements in hypocentral accuracy, particularly in-depth resolution and spatial clustering. This enhanced resolution transformed the initially diffuse cloud of seismicity into sharply delineated, NW–SE-trending spheroid, predominantly confined with the Al-Idrissi–Trougout–Ras Tarf Fault network with most activity at ~3–20 km and a sparser tail to ~50–60 km. The cluster widths the BAIV structural high and lies immediately north of the subsiding Al Hoceima Bay, providing the structural framework.

Our merged and expanded dataset includes lower-magnitude events down to Mw 1.5, yielding a much denser and more resolved image of the swarm's internal architecture, likely triggering processes, and spatiotemporal evolution. In contrast to earlier works of Lozano et al., (2025), who analyzed a limited set of moderate events drawn exclusively from the IGN catalogue, and Bouhali et al., (2025), who offered a broader swarm-scale overview based solely on the CNRST catalogue. Our combined catalogue leverages complementary coverage and improves depth control and event linkage. The relocated seismicity delineates a steep, near-vertical, NE–SW–aligned column that we interpret as a seismogenic conduit linking the brittle upper crust to deeper lithospheric levels (to ~60 km), situated within the Al-Idrissi–Trougout–Ras Tarf network and plausibly influenced by long-lived magmatic and volcanic features in the area (e.g. BAIV; Lafosse et al., 2020), including the

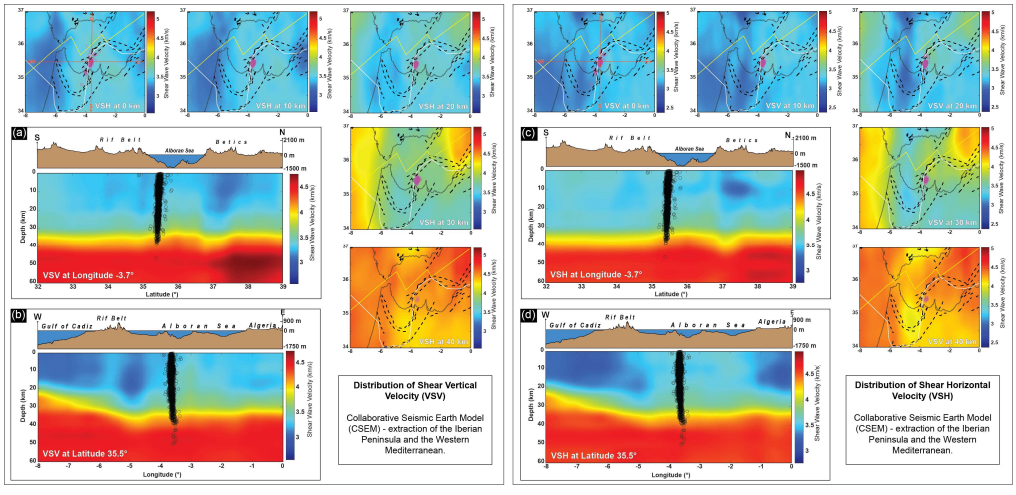

Figure 10: Shear wave velocity structure from the Collaborative Seismic Earth Model (CSEM), illustrating horizontal (VSH) and vertical (VSV) shear velocity variations across the Alboran region and Western Mediterranean. Depth slices at 10 km intervals down to 40 km, along with cross-sections at longitude -3.7° and latitude 35.5°, reveal velocity variations. Active fault zones (black doted lines) and (Black circles) relocated combined catalogue, yellow and white lines represent plate boundaries from (Coffin et al., 1998) and (Bird, 2003), respectively.

https://doi.org/10.5194/egusphere-2025-6433
Preprint. Discussion started: 21 April 2026

Ras Tarf volcanic field (9.0–4.8 Ma; El Azzouzi et al., 2014) and the Alboran Ridge (7.5–18.2 Ma; Duggen et al., 2004), which together suggest persistent deep pathways that can facilitate fluid transfer. Importantly, the column includes a sharp lithologic and rigidity contrast where the BAIV volcanic basement and exhumed Alboran-type crust to the N-NE neighbour a thicker Plio–Quaternary sedimentary pile within the subsiding Al Hoceima trough to the S-SW; this juxtaposition of stiff, higher-velocity basement against weaker, lower-velocity sediments focuses strain and helps explain the change in fault azimuth and curvature across the Bokkoya–AIFZ–Ras Tarf–Trougout relay, where mapped segments "turn" and step to form local releasing bends (Fig. 11) (Lafosse et al., 2020; Martínez-García et al., 2013). These findings are consistent with prior marine-geophysical, tomographic, and tectonic studies that document crustal thinning, a highly fractured upper crust, mantle upwelling, and fluid involvement across the western Alboran domain (e.g., Fullea et al., 2010; Galindo-Zaldivar et al., 2018; Gómez de la Peña et al., 2018; Martínez-García et al., 2013; Seber et al., 1996; Torne et al., 2000). Moreover, comparison with swarms in analogous transtensional settings shows similar diagnostics (compact vertical columns, migration in depth–time and distance–time space, b-values near 1, mixed strike-slip with minor normal components), supporting a stress-driven, fault-controlled sequence that is likely modulated by fluids, consistent with the southward maturation of the AIFS.

5.1. Tectonic Architecture and Fault System Dynamics of the Alboran Region

The Alboran Basin and the adjoining Rif–Betic belts sit within a diffuse Nubia–Eurasia boundary where oblique convergence is partitioned onto a hierarchically organized network of inherited and active faults with dominant strike-slip and transtensional kinematics (Gràcia et al., 2006; Koulali et al., 2011; Sanz de Galdeano et al., 2019; Stich et al., 2020; Tahayt et al., 2009; Tendero-Salmerón et al., 2022). Within this framework, the TASZ links major segments from Carboneras in the north to the Yusuf, Al-Idrissi and Alboran Ridge systems in the south, forming a broad corridor that accommodates oblique plate motion (Perea et al., 2018; Somoza et al., 2021).

Recent marine work emphasizes that the AIFS is an actively growing, left-lateral system that has propagated over the last ~1–1.8 Ma, linking through the Small Al-Idrissi Volcano (SAIV) into the Bokkoya Fault System and potentially maturing into an intra-continental plate-boundary strand (d'Acremont et al., 2020; Galindo-Zaldivar et al., 2018; Gràcia et al., 2019; Lafosse et al., 2020). Vidil et al., (2025b) explicitly document this relay architecture, with SAIV acting as the transfer zone between the Al-Idrissi and Bokkoya systems, while BAIV mapped as a topographic structural high within the same network, and AIFS segments showing mixed strike-slip with local transpression/transtension consistent with GPS and morpho-structural data (Lafosse et al., 2020; Vidil et al., 2025b). Along the northern Bokkoya segment, Vidil et al., (2025b) identify ~3 km of horizontal offset of the SAIV magmatic basement from bathymetry and seismic reflection, implying sustained Plio–Quaternary strike-slip with a minor normal component and step-over behaviour that concentrates strain and vertical throws locally (Vidil et al., 2025b). Additional marine-geophysical evidence along southern AIFS/Bokkoya and adjacent relays documents recurrent late-Quaternary faulting and seafloor instabilities (offset reflectors, disrupted contourites, canyon-flank scarps, and slope-failure deposits) that are compatible with cumulative vertical throw on active segments and repeated strong-shaking episodes (d'Acremont et al., 2020; Lafosse et al., 2020; Tendero-Salmerón et al., 2022). These segments juxtapose volcanic basement (chaotic, high-amplitude magmatic facies) against well-bedded sedimentary packages, sharpening lateral contrasts in rigidity and permeability where faults bend and link (Calvert et al., 2000). Consistently, seismic sections from (Vidil et al., 2025b) show magmatic basement with chaotic/transparent facies capped by abraded summit plateaus on BAIV/Alboran Ridge at ~110 mbsl, and a more rugged, deeper SAIV summit, features characteristic of long-lived structural highs that focus strain and channel fluid pathways along their flanks (Duggen et al., 2004; Lafosse et al., 2020; Vidil et al., 2025b).

Against this regional template, our results place the 2021–2022 sequence squarely within the NE–SW corridor defined by the southern AIFZ, the Trougout Fault, and the Ras Tarf (F1) segment (see Fig. 2 and 9). The swarm focal mechanisms remain dominantly strike-slip with minor normal components, kinematically consistent with the oblique ENE–WSW shortening/NNW–SSE extension field and the releasing geometries expected at step-overs and segment tips (Akoglu et al.,

https://doi.org/10.5194/egusphere-2025-6433
Preprint. Discussion started: 21 April 2026

2006; Kariche et al., 2018; Medina and Cherkaoui, 2017; Peláez et al., 2018; Stich et al., 2005). The 2016 crisis helped clarify the AIFS geometry and its onshore linkages (Bokkoya, Trougout, Nekor), and since 2016 seismicity has migrated toward the Trougout sector, consistent with evolving segment connectivity and stress transfer through bends/step-overs (Akka et al., 2024; Gràcia et al., 2019; Olaiz et al., 2025; Stich et al., 2020). Lozano et al., (2025) complement this view by relocating the 2016

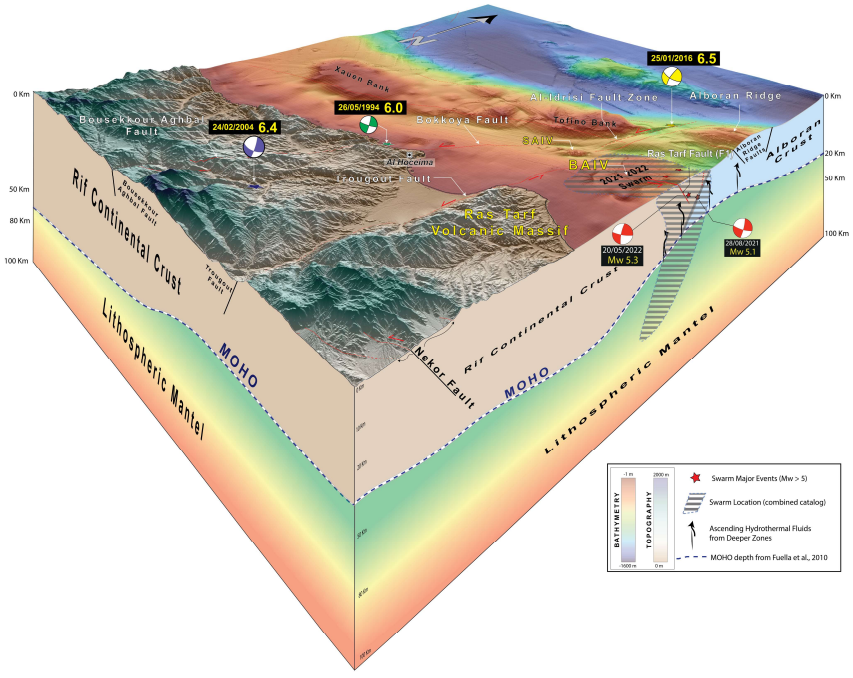

Figure 11: Three-dimensional lithospheric model of the Rif–Alboran region highlighting the tectonic and geodynamic context of the 2021–2022 seismic swarm. The model displays major fault systems, including the Al-Idrissi Fault Zone, Trougout Fault, and Ras Tarf Fault (F1). Relocated seismic events from the combined catalogue are shown along with focal mechanisms of mainshock events (Mw > 5, marked by red stars). Black arrows represent inferred pathways of deep fluid migration. Moho depth is based on the model of Fullea et al. (2010).

and 2021 activity to the western and eastern limits of AIFS, respectively, and arguing that the 2021 series may have activated an unmapped AIFS structure; they also highlight the predominance of shallow, low-to-moderate magnitudes in 2021 consistent with swarm-type, distributed slip rather than a single mainshock rupture. In parallel, (Bouhali et al., 2025) use kernel densities of events and seismic moment (computed over a wide Alboran domain) to show peak clustering and energy release along the Alboran Ridge–Central Rif belt that includes the AIFS, and b-values near the southern AIFS, consistent with slip-dominated behaviour. Together with Vidil et al., (2025b) documentation of active relays and mixed kinematics at SAIV–Bokkoya, these external constraints match our relocated geometry and mechanism mix: the swarm exploited pre-existing, high-angle strike-slip segments within a structurally complex relay where volcanic highs (BAIV/SAIV) bound sedimentary lows, local step-overs add small normal components, and segment tips steer along-strike migration (d'Acremont et al., 2020; Lafosse et al., 2020; Vidil et al., 2025b).

Finally, we note that BAIV/SAIV provide a natural locus for fault turning and linkage where volcanic basement and sedimentary basins meet. Vidil et al., (2025b) show that the SAIV–Bokkoya transition exhibits evidence of tensile step-over behaviour and possibly creeping-like deformation in low-M activity. An observation consistent with models in which young, narrow step-overs permit only short rupture jumps and redistribute strain off-fault (Cuba, 2023; Lozos, 2013; Ryan and Oglesby, 2014). In this sense, the post-2016 northeast-ward drift of seismicity and the 2021–2022 swarm concentration near the AIFZ–Trougout–Ras Tarf (F1) triple junction reflect the expected evolution of a propagating left-lateral system: slip partitions onto conjugate sets, bends/relays localize mixed kinematics, and the strongest contrasts in lithology and mechanical

https://doi.org/10.5194/egusphere-2025-6433
Preprint. Discussion started: 21 April 2026

properties (volcanic highs vs. fault-bounded lows) dictate where swarms can nucleate and persist (Bouhali et al., 2025; d'Acremont et al., 2020; Fernández-Ibáñez and Soto, 2008; Lozano et al., 2025; Platt and Vissers, 1989; Vidil et al., 2025b).

5.2. Fluid Influence on Swarm Dynamics and Triggering Mechanisms

Seismic tomography and crustal-thickness models indicate a locally attenuated lithosphere in the western Alboran domain, with thin crust and shallow Moho depths (on the order of ~14–22 km and ~25 km, respectively), consistent with prolonged stretching, slab delamination, and thermal weakening (Booth-Rea et al., 2007; Fernández-Ibáñez and Soto, 2008; Fullea et al., 2010; de Lis Mancilla et al., 2015; Platt and Vissers, 1989; Thurner et al., 2014; Villaseñor et al., 2015). Coeval Neogene to recent volcanism (e.g., Ras Tarf, Alboran Ridge) attests to sustained mantle-derived inputs (El Azzouzi et al., 2014; Duggen et al., 2004), and such systems are recognized sources of CO_2–H_2O–rich fluids capable of migrating upward through fracture networks (Giggenbach, 1992; Manning, 2004; Wallace, 2005). In a crust already segmented by inherited and active faults, this geodynamic context favours vertical fluid transport and permeability anisotropy (Hainzl et al., 2012; Juncu et al., 2017; Sibson, 1996). The configuration discussed above, elevated, fractured volcanic basement at BAIV, further sharpens lateral contrasts in rigidity and permeability and helps localize pathways along the AIFZ–Trougout– Ras Tarf (F1) relay (d'Acremont et al., 2020; Lafosse, M., Boutoux, A., Bellahsen, N. and Le Pourhiet, 2016; Lafosse et al., 2020).

Within this framework, fluids are a plausible modulating factor for the 2021–2022 sequence. Episodic increases in pore pressure can reduce effective normal stress, promote slow slip/creep on favourably oriented segments, and organize swarm-like seismic release (Cornelio et al., 2019; Hainzl et al., 2012; Leptokaropoulos et al., 2023; Sibson, 1996). Observationally, low seismicity and a low, continuous vertical slip rate along the Bokkoya reach are consistent with creeping-prone behaviour in parts of the network (Vidil et al., 2025b), while laboratory and modelling studies show that fluid lubrication can damp dynamic rupture and favour stable or occasionally unstable sliding (Cornelio et al., 2019; Fabbri et al., 2024). Field analogues from damaged crustal settings likewise link hydrothermal circulation to smaller magnitudes and enhanced aseismic slip (Leptokaropoulos et al., 2023). These behaviours are compatible with the relay geometry and stepovers mapped across the southern AIFZ, where short, young bends often redistribute strain off-fault and limit through-going rupture.

Our results fit this picture in space and time. The combined relocation yields a steep, vertically connected column of seismicity (Figs. 9–10) that evolves in episodic bursts (Fig. 8). Depth–time and distance–time diagnostics show an initial downward migration followed by upward propagation and a vertically confined distribution, a three-stage sequence that is consistent with alternating stress loading and fluid-pressure pulses. Inversion of the space–time migration yields apparent seismic diffusivities of ~1.2–13.9 $m^2\ s^{-1}$, within the upper range reported for recognized fluid-modulated swarms in geothermal/volcanic systems (Hainzl et al., 2012; Prejean et al., 2002; Shelly et al., 2015). Within this diffusivity envelope, seismicity is released in discrete bursts whose migration fronts advance several kilometres per day (~3–4.5 km day^{-1}; Fig. 8), implying a transient, localized acceleration of strain release during each episode. The recurrent upward phases over ~7–15 days are in line with discrete fluid-pressure fronts (Shelly, 2024), and cyclic variations in Gutenberg–Richter b-values further indicate transient, short-wavelength changes in effective stress and fault strength (Manga and Brodsky, 2006; Tormann et al., 2014; Wiemer and Wyss, 2000). At depth, shear-wave tomography shows velocity anomalies between ~30 and 70 km (VSH/VSV) consistent with partially serpentinized mantle and/or the margins of a delaminating slab (Bezacier et al., 2010; Fullea et al., 2010; Hacker et al., 2003; Sibson, 1996; Villaseñor et al., 2015). These low-velocity domains lie near the base of the vertical seismic column (Fig. 10), providing a plausible deep source and conduit for fluids. In this sense, the swarm behaviour is well described by a fault-valve process (Sibson, 1996): high-pressure fluids episodically breach sealed patches, generate clustered failure until pressure drops, and then re-seal, naturally producing bursty release and short-period migration.

In sum, the 2021–2022 sequence is best understood as the time-dependent expression of slip partitioning within a distributed, internally deforming Nubia–Eurasia boundary (Bird, 2003; Coffin et al., 1998; Somoza et al., 2021), where the Rif–Alboran domain behaves block-like under oblique convergence and rotation (Palano et al., 2013; Palomeras et al., 2014; Serpelloni et

https://doi.org/10.5194/egusphere-2025-6433
Preprint. Discussion started: 21 April 2026

al., 2007). The thin, mechanically attenuated lithosphere (Booth-Rea et al., 2007; Fullea et al., 2010; de Lis Mancilla et al., 2015; Thurner et al., 2014; Villaseñor et al., 2015) and the relay of inherited, steep strike-slip segments along TASZ–AIFZ–Trougout focus strain into the narrow BAIV–Ras Tarf (F1) corridor. Within this context, BAIV acts as a lateral seismogenic boundary, a partial barrier to through-going rupture and fluid diffusion, while the adjacent graben of Al Hoceima provides a mechanically weaker, permeable low, together steering where seismicity can nucleate, migrate, and stop (d'Acremont et al., 2020; Lafosse et al., 2020; Vidil et al., 2025b). The conjunction of episodic upward migration, elevated diffusivities, and lower-crust to upper-mantle velocity anomalies argues that fluids are a probable and modulating influence, but not a uniquely causal one; tectonic stressing, stress transfer across bends, and local aseismic slip likely co-govern the swarm evolution (Danré et al., 2019; Hainzl et al., 2012; Hainzl and Ogata, 2005; Im and Avouac, 2023; Marsan and Lengliné, 2008; Prejean et al., 2002; Shelly et al., 2007, 2015; Sibson, 1996; Uchida and Bürgmann, 2019; Vidale and Shearer, 2006). Framed this way, the Alboran swarm does not require new structures or a change in regional stress, it reflects ongoing transtensional partitioning on pre-existing faults within a strong–weak block mosaic, in which velocity gradients, lithologic juxtapositions (volcanic basement vs. sedimentary trough), and relay geometry set the boundaries of rupture and the pathways for pressure transients. This integrated view aligns the relocation, focal mechanisms, RT/diffusivity, and tomography, and provides testable expectations for future sequences. Swarms should preferentially recur where strong blocks bound weak corridors, notably at the BAIV–Ras Tarf (F1)–Bokkoya–Trougout junction, and their temporal clustering should be sensitive to the evolving balance between tectonic loading and episodic fluid access to the fault network. (Ben-Zion and Sammis, 2003; Civiero et al., 2019, 2020; Hainzl et al., 2012; Manga and Brodsky, 2006; Palomeras et al., 2014; Parotidis et al., 2004; Shapiro et al., 1997; Shelly et al., 2013, 2015; Sibson, 1996; Vidil et al., 2025b).

6. Conclusions

This study refines the geometry, kinematics, and deep context of the 2021–2022 South Alboran Sea, shedding light on the complex interplay between tectonic stress, fluid role, and inherited fault structures within a diffuse plate boundary zone. Our multi-disciplinary approach, combining earthquake bulletins, relocation with *HypoInverse* and *HypoDD*, focal mechanism analysis, spatiotemporal migration tracking, and integration with geophysical and geological morphotectonics data, yields several key findings with broader implications for the tectonic evolution and seismic hazard of the western Mediterranean region.

1. Using a regionally adapted 1-D model, *HypoInverse* located 5,285/5,330 matched events and *HypoDD* relocated 3,525 of them in the merged catalogue (CNRST: 2,124; IGN: 1,820). Median RMS for *HypoInverse* was ~0.18–0.25s; for HypoDD ~0.36–0.39s. Reported location uncertainties are ~2.1–4.1 km (*HypoInverse*) and ~7.8–9.7 km (*HypoDD*), as expected for a double-difference solution that optimizes relative geometry within clusters while absolute errors remain controlled by station layout and cross-network heterogeneity. The merged solution tightens a diffuse cloud into a narrow, NNE–SSW/NE–SW–aligned column with most activity at ~10–25 km depth (tail to ~50–60 km depth), squarely within the Al-Idrissi–Trougout–Ras Tarf (F1) relay on the flank of the Big Al-Idrissi Volcano (BAIV) and just north of the subsiding Al Hoceima Bay.
2. Depth–time and magnitude–time diagnostics show repeated bursts initiated by moderate events (e.g., Mw 4.7 on 07-Aug-2021; Mw 5.2 on 23-Dec-2021; Mw 5.0 on 20-May-2022; Mw 4.4 on 04-Oct-2022) followed by dense Mw $\lesssim$ 3.5 sequences at similar depths. Relocation removed events with 0-km depth fixes and consolidated activity into a recurrent ~10–20 km depth band. The persistence of a magnitude ceiling ($\leq$ Mw ~5) and the mid- to upper-crustal depth range point to intermittent reactivation of existing, steep strike-slip segments rather than progressive loading toward a larger mainshock.

https://doi.org/10.5194/egusphere-2025-6433
Preprint. Discussion started: 21 April 2026

3. Spatiotemporal evolution of the swarm exhibits a three-stage pattern: initial downward propagation, upward migration, and final vertical confinement, coupled with fluid diffusivity estimates ranging from 1.2 to 13.9 m^2/s. These values fall within the upper range of global fluid-induced swarm analogues (e.g., Yellowstone, Vogtland), supporting the hypothesis that fluid overpressure plays a critical role in swarm initiation, rather than purely tectonic stress. The seismic behaviour observed is consistent with pore-pressure diffusion and "fault-valve" dynamics.
4. Radius-time (RT) envelopes yield apparent diffusivities of ~1.2–13.9 $m^2\ s^{-1}$, within upper ranges reported for fluid-modulated swarms. Together with cyclic burst timing, upward phases, and the tomography-derived weak corridor, this supports fluid involvement as a timing/strength modulator superimposed on ongoing transtensional loading. At the same time, stress transfer across bends/step-overs and possible slow slip/creep on parts of the network (e.g., AIFZ, Ras Tarf (F1), Bokkoya) likely co-govern the sequence.
5. Focal mechanisms (IGN) cluster in the strike-slip field; nodal planes parallel the AIFZ/ Ras Tarf (F1) grain (NE–SW), with minor normal components concentrated at bends and segment tips, consistent with the oblique ENE–WSW shortening/NNW–SSE extension field and the relay geometry at the AIFZ–Trougout–Ras Tarf (F1) junction.
6. CSEM Iberia-2019 VSH/VSV slices show a NE–SW shallow low-V corridor (~3.0–3.5 km s^{-1}) co-linear with AIFZ/Yusuf/ Ras Tarf (F1) and overlying BAIV, abutting a faster lower-crustal "lid" (~4.3–4.7 km s^{-1}). Seismicity, this swarm included, clusters along the margins of faster blocks rather than within uniformly low-V areas, underscoring the role of velocity gradients (i.e., rigidity contrasts) in focusing strain onto bordering, below-resolution faults. At depth (≈30–70 km), mantle/lower-crust anomalies at the base of the column provide a plausible connection to deeper sources and pathways. Along with the spatial correlation with Miocene to Quaternary volcanic structures (e.g., Ras Tarf, Alboran Ridge) could supports a mantle-derived origin of fluids feeding into crustal fault systems.
7. The juxtaposition of an elevated, fractured volcanic basement (BAIV) against a subsiding, sediment-filled trough (Al Hoceima) imposes sharp lateral contrasts in rigidity and permeability. In this setting, the BAIV–Ras Tarf (F1)–Bokkoya–Trougout relay provides the preferred, high-permeability/high-stress-gradient path for swarm nucleation and along-strike migration, while BAIV plausibly limits through-going rupture and fluid diffusion laterally.

The 2021–2022 seismic swarm in the South Alboran Sea is emblematic of the tectonic complexity and dynamic behaviour of diffuse plate boundaries. It demonstrates how inherited structures, lithospheric conditions, and fluid migration processes can collectively shape seismicity. The swarm is best understood as the time-dependent expression of slip partitioning within a distributed Nubia–Eurasia boundary: intermittent reactivation of inherited AIFZ–Trougout–Ras Tarf (F1) segments within a strong–weak block mosaic, with fluids modulating when (and how intensely) clusters release. The stable magnitude ceiling in 2021–2022 is encouraging, yet the hierarchical, segmented architecture that favours swarms can also host larger ruptures under different loading/pressure histories. Priority actions include sustained cross-border seismic and geodetic coverage (onshore + OBS), routine catalogue harmonization/relocation, and coupled hydro-mechanical modelling targeted at the BAIV–Ras Tarf (F1)–Bokkoya–Trougout junction to evaluate evolving hazard within this corridor. Despite the extensive seismic activity and moment release during the 2021–2022 swarm, a notable strain deficit persists. This raises the possibility of future moderate to large earthquakes in the region, particularly if fluid pressure temporarily stabilizes and tectonic stress accumulates. The hierarchical nature of faulting and the observed vertical linkage between deep and shallow seismicity also indicate that rupture could propagate across multiple Fault segments scales. These characteristics, together with the fluid-sensitive behaviour of fault zones, underscore the need for continuous, high-resolution monitoring networks and coupled hydro-mechanical modelling to better anticipate swarm behaviour and earthquake potential.

Code and data availability

The code and data used in this study are available from the corresponding author upon reasonable request.

https://doi.org/10.5194/egusphere-2025-6433
Preprint. Discussion started: 21 April 2026

Author contributions

AH conceptualized the study, prepared the datasets, carried out the modelling and analysis, and wrote the manuscript. RA contributed to the conceptualization of the study and to the review and editing of the manuscript. TA contributed to the conceptualization of the study and to the review and editing of the manuscript.

Competing interests

The authors declare that they have no conflict of interest.

Acknowledgements

We would like to express our gratitude to CNRST (Morocco) and IGN (Spain) for providing the seismic bulletins and catalogues. We also acknowledge the support of our home institutions and laboratories, which provided the research environment and infrastructure necessary to carry out this study.

Financial support

This work was supported by the PHC Toubkal Hubert Curien Partenariat programme (Campus France–CNRST), project PHC Toubkal/24/197 (Campus France 50018WL).

References

Akka, H., Tahayt, A., Es-Sabbar, I., Ouammou, H., Jabour, N., and d'Acremont, E.: Evidence of Seismic Gap in Al Hoceima (Morocco): Implication for Seismic Hazard, in: Advances in Science, Technology and Innovation, 257–261, https://doi.org/10.1007/978-3-031-48715-6_56, 2024.

Akoglu, A. M., Cakir, Z., Meghraoui, M., Belabbes, S., El Alami, S. O., Ergintav, S., and Akyüz, H. S.: The 1994-2004 Al Hoceima (Morocco) earthquake sequence: Conjugate fault ruptures deduced from InSAR, Earth Planet. Sci. Lett., 252, 467–480, https://doi.org/10.1016/j.epsl.2006.10.010, 2006.

El Alami, S. O., Tadili, B. A., Cherkaoui, T.-E., Medina, F., Ramdani, M., Brahim, L. A., and Harnafi, M.: The Al Hoceima earthquake of May 26, 1994 and its aftershocks: a seismotectonic study, Ann. Geophys., 41, https://doi.org/10.4401/ag-3801, 1998.

Álvarez-Gómez, J. A.: FMC—Earthquake focal mechanisms data management, cluster and classification, SoftwareX, 9, 299–307, https://doi.org/10.1016/j.softx.2019.03.008, 2019.

Arroucau, P., Custódio, S., Civiero, C., Silveira, G., Dias, N., Díaz, J., Villaseñor, A., and Bodin, T.: PRISM3D: A 3-D reference seismic model for Iberia and adjacent areas, Geophys. J. Int., 225, 789–810, https://doi.org/10.1093/gji/ggab005, 2021.

El Azzouzi, M., Bellon, H., Coutelle, A., and Réhault, J. P.: Miocene magmatism and tectonics within the Peri-Alboran orogen (western Mediterranean), J. Geodyn., 77, 171–185, https://doi.org/10.1016/j.jog.2014.02.006, 2014.

Baratin, L.-M., Mazzotti, S., Chéry, J., Vernant, P., Tahayt, A., and Mourabit, T.: Incipient mantle delamination, active tectonics and crustal thickening in Northern Morocco: Insights from gravity data and numerical modeling, Earth Planet. Sci. Lett., 454, 113–120, https://doi.org/10.1016/j.epsl.2016.08.041, 2016.

De Barros, L., Baques, M., Godano, M., Helmstetter, A., Deschamps, A., Larroque, C., and Courboulex, F.: Fluid-induced

https://doi.org/10.5194/egusphere-2025-6433
Preprint. Discussion started: 21 April 2026

swarms and coseismic stress transfer: A dual process highlighted in the aftershock sequence of the 7 April 2014 earthquake (Ml 4.8, Ubaye, France), J. Geophys. Res. Solid Earth, 124, 3918–3932, https://doi.org/10.1029/2018JB017226, 2019.

Ben-Zion, Y. and Sammis, C. G.: Characterization of fault zones, Pure Appl. Geophys., 160, 677–715, https://doi.org/10.1007/PL00012554, 2003.

Bezacier, L., Reynard, B., Bass, J. D., Wang, J., and Mainprice, D.: Elasticity of glaucophane, seismic velocities and anisotropy of the subducted oceanic crust, Tectonophysics, 494, 201–210, https://doi.org/10.1016/j.tecto.2010.09.011, 2010.

Bezada, M. J. and Humphreys, E. D.: Contrasting rupture processes during the April 11, 2010 deep-focus earthquake beneath Granada, Spain, Earth Planet. Sci. Lett., 353, 38–46, https://doi.org/10.1016/j.epsl.2012.08.001, 2012.

Bezada, M. J., Humphreys, E. D., Toomey, D. R., Harnafi, M., Dávila, J. M., and Gallart, J.: Evidence for slab rollback in westernmost Mediterranean from improved upper mantle imaging, Earth Planet. Sci. Lett., 368, 51–60, https://doi.org/10.1016/j.epsl.2013.02.024, 2013.

Bezzeghoud, M. and Buforn, E.: Source parameters of the 1992 Melilla (Spain, MW = 4.8), 1994 Alhoceima (Morocco, MW = 5.8), and 1994 Mascara (Algeria, MW = 5.7) earthquakes and seismotectonic implications, Bull. Seismol. Soc. Am., 89, 359–372, https://doi.org/10.1785/bssa0890020359, 1999.

Biggs, J., Bergman, E., Emmerson, B., Funning, G. J., Jackson, J., Parsons, B., and Wright, T. J.: Fault identification for buried strike-slip earthquakes using InSAR: The 1994 and 2004 Al Hoceima, Morocco earthquakes, Geophys. J. Int., 166, 1347–1362, https://doi.org/10.1111/j.1365-246X.2006.03071.x, 2006.

Bird, P.: An updated digital model of plate boundaries, Geochemistry, Geophys. Geosystems, 4, https://doi.org/10.1029/2001GC000252, 2003.

Blanco, M. J. and Spakman, W.: The P-wave velocity structure of the mantle below the Iberian Peninsula: evidence for subducted lithosphere below southern Spain, Tectonophysics, 221, 13–34, https://doi.org/10.1016/0040-1951(93)90025-F, 1993.

Blinova, V. N., Comas, M. C., Ivanov, M. K., Poludetkina, E. N., and Matveeva, T. V: Active mud volcanism in the West Alboran Basin: Geochemical evidence of hydrocarbon seepage, Mar. Pet. Geol., 28, 1483–1504, https://doi.org/10.1016/j.marpetgeo.2011.06.001, 2011.

Bondár, I., Myers, S. C., Engdahl, E. R., and Bergman, E. A.: Epicentre accuracy based on seismic network criteria, Geophys. J. Int., 156, 483–496, https://doi.org/10.1111/j.1365-246X.2004.02070.x, 2004.

Booth-Rea, G., Ranero, C. R., Grevemeyer, I., and Martínez-Martínez, J. M.: Crustal types and tertiary tectonic evolution of the Alborán sea, western Mediterranean, Geochemistry, Geophys. Geosystems, 8, https://doi.org/10.1029/2007GC001639, 2007.

Bouhali, K., Rouai, M., Dekayir, A., and Essaied, A.: The South Alboran Basin Seismic Swarm in 2020-2021 and its Possible Relation to the Southern Development of the Al-Idrissi Fault System, Геодинамика и тектонофизика, 16, 9, https://doi.org/10.5800/GT-2025-16-1-0804, 2025.

Buforn, E., De Galdeano, C. S., and Udías, A.: Seismotectonics of the Ibero-Maghrebian region, Tectonophysics, 248, 247–261, https://doi.org/10.1016/0040-1951(94)00276-F, 1995.

Buforn, E., Pro, C., Cesca, S., Udías, A., and Del Fresno, C.: The 2010 Granada, Spain, deep earthquake, Bull. Seismol. Soc. Am., 101, 2418–2430, https://doi.org/10.1785/0120110022, 2011.

Buforn, E., Pro, C., Sanz de Galdeano, C., Cantavella, J. V., Cesca, S., Caldeira, B., Udías, A., and Mattesini, M.: The 2016 south Alboran earthquake (Mw = 6.4): A reactivation of the Ibero-Maghrebian region?, Tectonophysics, 712–713, 704–715, https://doi.org/10.1016/j.tecto.2017.06.033, 2017.

Cakir, Z., Meghraoui, M., Akoglu, A. M., Jabour, N., Belabbes, S., and Ait-Brahim, L.: Surface deformation associated with the M w 6.4, 24 February 2004 Al Hoceima, Morocco, earthquake deduced from InSAR: Implications for the active tectonics along North Africa, Bull. Seismol. Soc. Am., 96, 59–68, https://doi.org/10.1785/0120050108, 2006.

https://doi.org/10.5194/egusphere-2025-6433
Preprint. Discussion started: 21 April 2026

Calvert, A., Sandvol, E., Seber, D., Barazangi, M., Roecker, S., Mourabit, T., Vidal, F., Alguacil, G., and Jabour, N.: Geodynamic evolution of the lithosphere and upper mantle beneath the Alboran region of the western Mediterranean: Constraints from travel time tomography, J. Geophys. Res. Solid Earth, 105, 10871–10898, https://doi.org/10.1029/2000jb900024, 2000.

Cattania, C. and Segall, P.: Precursory slow slip and foreshocks on rough faults, J. Geophys. Res. Solid Earth, 126, https://doi.org/10.1029/2020JB020430, 2021.

Cavalcante, G. C. G., Viegas, G., Archanjo, C. J., and da Silva, M. E.: The influence of partial melting and melt migration on the rheology of the continental crust, J. Geodyn., 101, 186–199, https://doi.org/10.1016/j.jog.2016.06.002, 2016.

Civiero, C., Custódio, S., Rawlinson, N., Strak, V., Silveira, G., Arroucau, P., and Corela, C.: Thermal Nature of Mantle Upwellings Below the Ibero-Western Maghreb Region Inferred From Teleseismic Tomography, J. Geophys. Res. Solid Earth, 124, 1781–1801, https://doi.org/10.1029/2018JB016531, 2019.

Civiero, C., Custódio, S., Duarte, J. C., Mendes, V. B., and Faccenna, C.: Dynamics of the Gibraltar Arc System: A Complex Interaction Between Plate Convergence, Slab Pull, and Mantle Flow, J. Geophys. Res. Solid Earth, 125, https://doi.org/10.1029/2019JB018873, 2020.

Coffin, M. F. F., Gahagan, L. M. M., and Lawver, L. A. A.: Present-day Plate Boundary Digital Data Compilation, Univ. Texas Inst. Geophys. Tech. Rep., 174, 5, 1998.

Cornelio, C., Spagnuolo, E., Di Toro, G., Nielsen, S., and Violay, M.: Mechanical behaviour of fluid-lubricated faults, Nat. Commun., 10, 1274, https://doi.org/10.1038/s41467-019-09293-9, 2019.

Cox, S. F.: Injection-driven swarm seismicity and permeability enhancement: Implications for the dynamics of hydrothermal ore systems in high fluid-flux, overpressured faulting regimes - An invited paper, Econ. Geol., 111, 559–587, https://doi.org/10.2113/econgeo.111.3.559, 2016.

Cuba, J. F.: Earthquake rupture around stepovers in a brittle damage medium, 2023.

Custódio, S., Lima, V., Vales, D., Cesca, S., and Carrilho, F.: Imaging active faulting in a region of distributed deformation from the joint clustering of focal mechanisms and hypocentres: Application to the Azores-western Mediterranean region, Tectonophysics, 676, 70–89, https://doi.org/10.1016/j.tecto.2016.03.013, 2016.

d'Acremont, E., Gutscher, M.-A., Rabaute, A., de Lépinay, B. M., Lafosse, M., Poort, J., Ammar, A., Tahayt, A., Le Roy, P., and Smit, J.: High-resolution imagery of active faulting offshore Al Hoceima, Northern Morocco, Tectonophysics, 632, 160–166, https://doi.org/10.1016/j.tecto.2014.06.008, 2014.

d'Acremont, E., Lafosse, M., Rabaute, A., Teurquety, G., Do Couto, D., Ercilla, G., Juan, C., de Lépinay, B. M., Lafuerza, S., and Galindo-Zaldivar, J.: Polyphase tectonic evolution of fore-arc basin related to STEP fault as revealed by seismic reflection data from the Alboran Sea (W-Mediterranean), Tectonics, 39, https://doi.org/10.1029/2019TC005885, 2020.

Danre, P., De Barros, L., and Cappa, F.: A common model to explain similarities between injection-induced and natural earthquake swarms, in: EGU General Assembly Conference Abstracts, EGU21-1085, https://doi.org/10.5194/egusphere-egu21-1085, 2021.

Danré, P., Yin, J., Lipovsky, B. P., and Denolle, M. A.: Earthquakes Within Earthquakes: Patterns in Rupture Complexity, Geophys. Res. Lett., 46, 7352–7360, https://doi.org/10.1029/2019GL083093, 2019.

Díaz-Alvarado, J., González-Menéndez, L., Hidas, K., Azor, A., and Pedrera, A.: Tectono-metamorphic interaction of upper mantle peridotites and lower crustal units during continental rifting in the western Betic Cordillera, Gondwana Res., 132, 193–219, https://doi.org/10.1016/j.gr.2024.03.018, 2024.

Duarte, J. C., Riel, N., Civiero, C., Silva, S., Rosas, F. M., Schellart, W. P., Almeida, J., Terrinha, P., and Ribeiro, A.: Seismic evidence for oceanic plate delamination offshore Southwest Iberia, Nat. Geosci., 1–7, https://doi.org/10.1038/s41561-025-01781-6, 2025.

Duggen, S., Hoernle, K., van den Bogaard, P., and Harris, C.: Magmatic evolution of the Alboran region: The role of

https://doi.org/10.5194/egusphere-2025-6433
Preprint. Discussion started: 21 April 2026

subduction in forming the western Mediterranean and causing the Messinian Salinity Crisis, Earth Planet. Sci. Lett., 218, 91–108, https://doi.org/10.1016/S0012-821X(03)00632-0, 2004.

Fabbri, O., Raimbourg, H., and Leclère, H.: Fluids, faulting and earthquakes in the brittle crust: recent advances and new challenges, Comptes Rendus - Geosci., 356, 423–466, https://doi.org/10.5802/crgeos.259, 2024.

Faccenna, C., Piromallo, C., Crespo-Blanc, A., Jolivet, L., and Rossetti, F.: Lateral slab deformation and the origin of the western Mediterranean arcs, Tectonics, 23, https://doi.org/10.1029/2002TC001488, 2004.

Fadil, A., Vernant, P., McClusky, S., Reilinger, R., Gomez, F., Sari, D. Ben, Mourabit, T., Feigl, K., and Barazangi, M.: Active tectonics of the western Mediterranean: Geodetic evidence for rollback of a delaminated subcontinental lithospheric slab beneath the Rif Mountains, Morocco, Geology, 34, 529–532, https://doi.org/10.1130/G22291.1, 2006.

Faulkner, D. R., Jackson, C. A. L., Lunn, R. J., Schlische, R. W., Shipton, Z. K., Wibberley, C. A. J., and Withjack, M. O.: A review of recent developments concerning the structure, mechanics and fluid flow properties of fault zones, J. Struct. Geol., 32, 1557–1575, https://doi.org/10.1016/j.jsg.2010.06.009, 2010.

Fernández-Ibáñez, F. and Soto, J. I.: Crustal rheology and seismicity in the Gibraltar Arc (western Mediterranean), Tectonics, 27, https://doi.org/10.1029/2007TC002192, 2008.

Fullea, J., Fernàndez, M., Afonso, J. C., Vergés, J., and Zeyen, H.: The structure and evolution of the lithosphere-asthenosphere boundary beneath the Atlantic-Mediterranean Transition Region, Lithos, 120, 74–95, https://doi.org/10.1016/j.lithos.2010.03.003, 2010.

Galindo-Zaldivar, J., Ercilla, G., Estrada, F., Catalán, M., d'Acremont, E., Azzouz, O., Casas, D., Chourak, M., Vazquez, J. T., Chalouan, A., Sanz de Galdeano, C., Benmakhlouf, M., Gorini, C., Alonso, B., Palomino, D., Rengel, J. A., and Gil, A. J.: Imaging the Growth of Recent Faults: The Case of 2016–2017 Seismic Sequence Sea Bottom Deformation in the Alboran Sea (Western Mediterranean), Tectonics, 37, 2513–2530, https://doi.org/10.1029/2017TC004941, 2018.

Galindo-Zaldivar, J., Gil-Cruz, A. J., Azzouz, O., Ercilla, G., Sánchez-Alzola, A., de los Cobos, M. C., Ruiz-Armenteros, A. M., Bengamra, S., Estrada, F., and Ruano, P.: GPS tectonic displacements on a main active sinistral blind fault tip: a key to integrate seismic and geological evidences in a collisional setting (Al Hoceima area, Rif belt, western Mediterranean)., in: Geophysical Research Abstracts, 2019.

Galindo-Zaldívar, J., Azzouz, O., Chalouan, A., Pedrera, A., Ruano, P., Ruiz-Constán, A., de Galdeano, C. S., Marín-Lechado, C., López-Garrido, A. C., and Anahnah, F.: Extensional tectonics, graben development and fault terminations in the eastern Rif (Bokoya–Ras Afraou area), Tectonophysics, 663, 140–149, https://doi.org/10.1016/j.tecto.2015.08.029, 2015.

Gea, P. J., Negredo, A. M., and Mancilla, F. de L.: The Gibraltar slab dynamics and its influence on past and present-day Alboran domain deformation: Insights from thermo-mechanical numerical modelling, Front. Earth Sci., 11, 995041, https://doi.org/10.3389/feart.2023.995041, 2023.

Giammanco, S., Palano, M., Scaltrito, A., Scarfì, L., and Sortino, F.: Possible role of fluid overpressure in the generation of earthquake swarms in active tectonic areas: The case of the Peloritani Mts. (Sicily, Italy), J. Volcanol. Geotherm. Res., 178, 795–806, https://doi.org/10.1016/j.jvolgeores.2008.09.005, 2008.

Giggenbach, W. F.: Isotopic shifts in waters from geothermal and volcanic systems along convergent plate boundaries and their origin, Earth Planet. Sci. Lett., 113, 495–510, https://doi.org/10.1016/0012-821X(92)90127-H, 1992.

Gómez de la Peña, L., Ranero, C. R., and Gràcia, E.: The Crustal Domains of the Alboran Basin (Western Mediterranean), Tectonics, 37, 3352–3377, https://doi.org/10.1029/2017TC004946, 2018.

Gràcia, E., Pallàs, R., Soto, J. I., Comas, M., Moreno, X., Masana, E., Santanach, P., Diez, S., García, M., Dañobeitia, J., Bartolomé, R., Farrán, M., Gómez, M., Alpiste, M. J. R., Lastras, G., Wilmott, V., Perea, H., Blondel, P., Gómez, O., Bullock, L., Jacobs, C., Rouse, I., White, D., Whittle, S., Terrinha, P., Gafeira, J., and Roque, C.: Active faulting offshore SE Spain (Alboran Sea): Implications for earthquake hazard assessment in the Southern Iberian Margin, Earth Planet. Sci. Lett., 241, 734–749, https://doi.org/10.1016/j.epsl.2005.11.009, 2006.

https://doi.org/10.5194/egusphere-2025-6433
Preprint. Discussion started: 21 April 2026

Gràcia, E., Bartolomé, R., Lo Iacono, C., Moreno, X., Stich, D., Martínez-Díaz, J. J., Bozzano, G., Martínez-Loriente, S., Perea, H., and Diez, S.: Acoustic and seismic imaging of the Adra Fault (NE Alboran Sea): In search of the source of the 1910 Adra earthquake, Nat. Hazards Earth Syst. Sci., 12, 3255–3267, https://doi.org/10.5194/nhess-12-3255-2012, 2012.

Gràcia, E., Grevemeyer, I., Bartolomé, R., Perea, H., Martínez-Loriente, S., Gómez de la Peña, L., Villaseñor, A., Klinger, Y., Lo Iacono, C., Diez, S., Calahorrano, A., Camafort, M., Costa, S., d'Acremont, E., Rabaute, A., and Ranero, C. R.: Earthquake crisis unveils the growth of an incipient continental fault system, Nat. Commun., 10, 1–12, https://doi.org/10.1038/s41467-019-11064-5, 2019.

Grevemeyer, I., Gràcia, E., Villaseñor, A., Leuchters, W., and Watts, A. B.: Seismicity and active tectonics in the Alboran Sea, Western Mediterranean: Constraints from an offshore-onshore seismological network and swath bathymetry data, J. Geophys. Res. Solid Earth, 120, 8348–8365, https://doi.org/10.1002/2015JB012073, 2015.

Hacker, B. R., Peacock, S. M., Abers, G. A., and Holloway, S. D.: Subduction factory 2. Are intermediate-depth earthquakes in subducting slabs linked to metamorphic dehydration reactions?, J. Geophys. Res. Solid Earth, 108, https://doi.org/10.1029/2001jb001129, 2003.

Hainzl, S.: Seismicity patterns of earthquake swarms due to fluid intrusion and stress triggering, Geophys. J. Int., 159, 1090–1096, https://doi.org/10.1111/j.1365-246X.2004.02463.x, 2004.

Hainzl, S. and Ogata, Y.: Detecting fluid signals in seismicity data through statistical earthquake modeling, J. Geophys. Res. Solid Earth, 110, 1–10, https://doi.org/10.1029/2004JB003247, 2005.

Hainzl, S., Fischer, T., and Dahm, T.: Seismicity-based estimation of the driving fluid pressure in the case of swarm activity in Western Bohemia, Geophys. J. Int., 191, 271–281, https://doi.org/10.1111/j.1365-246X.2012.05610.x, 2012.

Harris, R. A.: Introduction to special section: Stress triggers, stress shadows, and implications for seismic hazard, https://doi.org/10.1029/98JB01576, 1998.

Hauksson, E. and Unruh, J.: Regional tectonics of the Coso geothermal area along the intracontinental plate boundary in central eastern California: Three-dimensional Vp and Vp/Vs models, spatial-temporal seismicity patterns, and seismogenic deformation, J. Geophys. Res. Solid Earth, 112, https://doi.org/10.1029/2006JB004721, 2007.

Hensen, C., Duarte, J. C., Vannucchi, P., Mazzini, A., Lever, M. A., Terrinha, P., Géli, L., Henry, P., Villinger, H., Morgan, J., Schmidt, M., Gutscher, M. A., Bartolome, R., Tomonaga, Y., Polonia, A., Gràcia, E., Tinivella, U., Lupi, M., Çağatay, M. N., Elvert, M., Sakellariou, D., Matias, L., Kipfer, R., Karageorgis, A. P., Ruffine, L., Liebetrau, V., Pierre, C., Schmidt, C., Batista, L., Gasperini, L., Burwicz, E., Neres, M., and Nuzzo, M.: Marine transform faults and fracture zones: A joint perspective integrating seismicity, fluid flow and life, Front. Earth Sci., 7, 1–29, https://doi.org/10.3389/feart.2019.00039, 2019.

Hill, D. P., Reasenberg, P. A., Michael, A., Arabaz, W. J., Beroza, G., Brumbaugh, D., Brune, J. N., Castro, R., Davis, S., and DePolo, D.: Seismicity remotely triggered by the magnitude 7.3 Landers, California, earthquake, Science (80-.)., 260, 1617–1623, https://doi.org/10.1126/science.260.5114.1617, 1993.

Husen, S. and Hardebeck, J.: Earthquake location accuracy, Community Online Resour. Stat. Seism. Anal., https://doi.org/10.5078/corssa-55815573, 2010.

Husen, S. and Smith, R. B.: Probabilistic earthquake relocation in three-dimensional velocity models for the Yellowstone National Park region, Wyoming, Bull. Seismol. Soc. Am., 94, 880–896, https://doi.org/10.1785/0120030170, 2004.

Ide, S.: Complex source processes and the interaction of moderate earthquakes during the earthquake swarm in the Hida-Mountains, Japan, 1998, Tectonophysics, 334, 35–54, https://doi.org/10.1016/S0040-1951(01)00027-0, 2001.

Im, K. and Avouac, J. P.: Cascading foreshocks, aftershocks and earthquake swarms in a discrete fault network, Geophys. J. Int., 235, 831–852, https://doi.org/10.1093/gji/ggad278, 2023.

Jousset, P., Haberland, C., Bauer, K., and Arnason, K.: Hengill geothermal volcanic complex (Iceland) characterized by integrated geophysical observations, Geothermics, 40, 1–24, https://doi.org/10.1016/j.geothermics.2010.12.008, 2011.

https://doi.org/10.5194/egusphere-2025-6433
Preprint. Discussion started: 21 April 2026

Juncu, D., Árnadóttir, T., Hooper, A., and Gunnarsson, G.: Anthropogenic and natural ground deformation in the Hengill geothermal area, Iceland, J. Geophys. Res. Solid Earth, 122, 692–709, https://doi.org/10.1002/2016JB013626, 2017.

Kariche, J., Meghraoui, M., Timoulali, Y., Cetin, E., and Toussaint, R.: The Al Hoceima earthquake sequence of 1994, 2004 and 2016: Stress transfer and poroelasticity in the Rif and Alboran Sea region, Geophys. J. Int., 212, 42–53, https://doi.org/10.1093/gji/ggx385, 2018.

Klein, F. W.: User's guide to HYPOINVERSE, a program for VAX computers to solve for earthquake locagtions and magnitudes, U.S. Geological Survey Open-File Report 89-314, US Geological Survey, 58 p pp., https://doi.org/10.3133/ofr89314, 1989.

Koulali, A., Ouazar, D., Tahayt, A., King, R. W., Vernant, P., Reilinger, R. E., McClusky, S., Mourabit, T., Davila, J. M., and Amraoui, N.: New GPS constraints on active deformation along the Africa-Iberia plate boundary, Earth Planet. Sci. Lett., 308, 211–217, https://doi.org/10.1016/j.epsl.2011.05.048, 2011.

Lafosse, M., Boutoux, A., Bellahsen, N. and Le Pourhiet, L.: Role of tectonic burial and temperature on the inversion of inherited extensional basins during collision, Geol. Mag., 153, 811–826, https://doi.org/10.1017/S0016756816000510, 2016.

Lafosse, M., D'Acremont, E., Rabaute, A., Estrada, F., Jollivet-Castelot, M., Vázquez, J. T., Galindo-Zaldivar, J., Ercilla, G., Alonso, B., Smit, J., Ammar, A., and Gorini, C.: Plio-Quaternary tectonic evolution of the southern margin of the Alboran Basin (Western Mediterranean), Solid Earth, 11, 741–765, https://doi.org/10.5194/se-11-741-2020, 2020.

Lee, W. H. . and Lahr J.C: HYPO71: a computer pro- gram for determining hypocenter, magnitude, and first motion pattern of local earthquakes, U.S. Geological Survey, US Dept. of the Interior, Geological Survey, National Center for Earthquake …, 100 pp., https://doi.org/10.3133/ofr72224, 1972.

Lengliné, O., Boubacar, M., and Schmittbuhl, J.: Seismicity related to the hydraulic stimulation of GRT1, Rittershoffen, France, Geophys. J. Int., 208, 1704–1715, https://doi.org/10.1093/gji/ggw490, 2017.

Leptokaropoulos, K., Rychert, C. A., Harmon, N., Schlaphorst, D., Grevemeyer, I., Kendall, J. M., and Singh, S. C.: Broad fault zones enable deep fluid transport and limit earthquake magnitudes, Nat. Commun., 14, 5748, https://doi.org/10.1038/s41467-023-41403-6, 2023.

de Lis Mancilla, F., Stich, D., Morales, J., Martín, R., Diaz, J., Pazos, A., Córdoba, D., Pulgar, J. A., Ibarra, P., Harnafi, M., and Gonzalez-Lodeiro, F.: Crustal thickness and images of the lithospheric discontinuities in the Gibraltar arc and surrounding areas, Geophys. J. Int., 203, 1804–1820, https://doi.org/10.1093/gji/ggv390, 2015.

de Lis Mancilla, F., Heit, B., Morales, J., Yuan, X., Stich, D., Molina-Aguilera, A., Azañon, J. M., and Martín, R.: A STEP fault in Central Betics, associated with lateral lithospheric tearing at the northern edge of the Gibraltar arc subduction system, Earth Planet. Sci. Lett., 486, 32–40, https://doi.org/10.1016/j.epsl.2018.01.008, 2018.

Lonergan, L. and White, N.: Origin of the Betic-Rif mountain belt, Tectonics, 16, 504–522, https://doi.org/10.1029/96TC03937, 1997.

Lozano, L., Buforn, E., Vicente Cantavella, J., López-Sánchez, C., Victoria Manzanedo, M., Barco, J., Antón, R., Cabieces, R., and Mattesini, M.: Relocation of Recent Shallow Seismic Activity in the Alboran Sea (Western Mediterranean Sea): The 2021–2024, 2016, and 2004 Seismic Series, Bull. Seismol. Soc. Am., 115, 469–488, https://doi.org/10.1785/0120240159, 2025.

Lozos, J. C.: Dynamic rupture and ground motion modeling on realistically complex strike-slip faults, University of California, Riverside, 2013.

Maestro-González, A., Bárcenas, P., Vázquez, J. T., and Díaz-del-Río, V.: The role of basement inheritance faults in the recent fracture system of the inner shelf around Alboran Island, Western Mediterranean, Geo-Marine Lett., 28, 53–64, https://doi.org/10.1007/s00367-007-0089-8, 2008.

Maiorana, M., Spatola, D., Todaro, S., Caldareri, F., Parente, F., Severini, A., and Sulli, A.: Seismo-stratigraphic and morpho-bathymetric analysis revealing recent fluid-rising phenomena on the Adventure Plateau (northwestern Sicily Channel), Mar.

https://doi.org/10.5194/egusphere-2025-6433
Preprint. Discussion started: 21 April 2026

Geophys. Res., 45, 15, https://doi.org/10.1007/s11001-024-09549-0, 2024.

Manga, M. and Brodsky, E.: Seismic triggering of eruptions in the far field: Volcanoes and geysers, Annu. Rev. Earth Planet. Sci., 34, 263–291, https://doi.org/10.1146/annurev.earth.34.031405.125125, 2006.

Manning, C. E.: The chemistry of subduction-zone fluids, Earth Planet. Sci. Lett., 223, 1–16, https://doi.org/10.1016/j.epsl.2004.04.030, 2004.

Marsan, D. and Lengliné, O.: Extending earthquakes' reach through cascading, Science (80-.)., 319, 1076–1079, https://doi.org/10.1126/science.1148783, 2008.

Martín, R., Stich, D., Morales, J., and Mancilla, F.: Moment tensor solutions for the Iberian-Maghreb region during the IberArray deployment (2009-2013), Tectonophysics, 663, 261–274, https://doi.org/10.1016/j.tecto.2015.08.012, 2015.

Martínez-García, P., Comas, M., Soto, J. I., Lonergan, L., and Watts, A. B.: Strike-slip tectonics and basin inversion in the western Mediterranean: the Post-Messinian evolution of the Alboran Sea, Basin Res., 25, 361–387, https://doi.org/10.1111/bre.12005, 2013.

Medialdea, T., Vegas, R., Somoza, L., Vázquez, J. T., Maldonado, A., Dıaz-del-Rıo, V., Maestro, A., Córdoba, D., and Fernández-Puga, M. C.: Structure and evolution of the "Olistostrome" complex of the Gibraltar Arc in the Gulf of Cádiz (eastern Central Atlantic): evidence from two long seismic cross-sections, Mar. Geol., 209, 173–198, https://doi.org/10.1016/j.margeo.2004.05.029, 2004.

Medina, F. and Cherkaoui, T.-E.: The South-Western Alboran Earthquake Sequence of January-March 2016 and Its Associated Coulomb Stress Changes, Open J. Earthq. Res., 06, 35–54, https://doi.org/10.4236/ojer.2017.61002, 2017.

El Moudnib, L., Villaseñor, A., Harnafi, M., Gallart, J., Pazos, A., Serrano, I., Córdoba, D., Pulgar, J. A., Ibarra, P., Himmi, M. M., and Chourak, M.: Crustal structure of the Betic-Rif system, western Mediterranean, from local earthquake tomography, Tectonophysics, 643, 94–105, https://doi.org/10.1016/j.tecto.2014.12.015, 2015.

Nakajima, J. and Hasegawa, A.: Prevalence of shallow low-frequency earthquakes in the continental crust, J. Geophys. Res. Solid Earth, 126, e2020JB021391, https://doi.org/10.1029/2020JB021391, 2021.

Negredo, A. M., Bird, P., Sanz de Galdeano, C., and Buforn, E.: Neotectonic modeling of the Ibero-Maghrebian region, J. Geophys. Res. Solid Earth, 107, ETG-10, https://doi.org/10.1029/2001JB000743, 2002.

Olaiz, A. J., Álvarez Gómez, J. A., de Vicente, G., Muñoz-Martín, A., Cantavella, J. V., Custódio, S., Vales, D., and Heidbach, O.: Seismo-tectonics of Greater Iberia: An updated review, Preprint, 2025, 1–108, https://doi.org/10.5194/egusphere-2024-4126, 2025.

Orange, D. L., Greene, H. G., Reed, D., Martin, J. B., McHugh, C. M., Ryan, W. B. F., Maher, N., Stakes, D., and Barry, J.: Widespread fluid expulsion on a translational continental margin: mud volcanoes, fault zones, headless canyons, and organic-rich substrate in Monterey Bay, California, Geol. Soc. Am. Bull., 111, 992–1009, https://doi.org/10.1130/0016-7606(1999)111<0992:WFEOAT>2.3.CO;2, 1999.

Oth, A.: On the characteristics of earthquake stress release variations in Japan, Earth Planet. Sci. Lett., 377, 132–141, https://doi.org/10.1016/j.epsl.2013.06.037, 2013.

Palano, M., González, P. J., and Fernández, J.: Strain and stress fields along the Gibraltar Orogenic Arc: Constraints on active geodynamics, Gondwana Res., 23, 1071–1088, https://doi.org/10.1016/j.gr.2012.05.021, 2013.

Palomeras, I., Thurner, S., Levander, A., Bezada, M., Villasenor, A., Humphreys, E., Carbonell, R., and Gallart, J.: Lithosphere and Asthenosphere Structure of the Western Mediterranean and Northwest Africa from Rayleigh Wave tomography and Ps Receiver Functions, in: EGU General Assembly Conference Abstracts, EGU2013-12324, 2013.

Palomeras, I., Thurner, S., Levander, A., Liu, K., Villaseñor, A., Carbonell, R., and Harnafi, M.: Finite-frequency Rayleigh wave tomography of the western Mediterranean: Mapping its lithospheric structure, Geochemistry, Geophys. Geosystems, 15, 140–160, https://doi.org/10.1002/2013GC004861, 2014.

Palomeras, I., Villaseñor, A., Thurner, S., Levander, A., Gallart, J., and Harnafi, M.: Lithospheric structure of Iberia and

https://doi.org/10.5194/egusphere-2025-6433
Preprint. Discussion started: 21 April 2026

Morocco using finite-frequency Rayleigh wave tomography from earthquakes and seismic ambient noise, Geochemistry, Geophys. Geosystems, 18, 1824–1840, https://doi.org/10.1002/2016GC006657, 2017.

Parotidis, M. and Shapiro, S. A.: A statistical model for the seismicity rate of fluid-injection-induced earthquakes, Geophys. Res. Lett., 31, https://doi.org/10.1029/2004GL020421, 2004.

Parotidis, M., Shapiro, S. A., and Rothert, E.: Back front of seismicity induced after termination of borehole fluid injection, Geophys. Res. Lett., 31, https://doi.org/10.1029/2003GL018987, 2004.

Parsons, T.: Global Omori law decay of triggered earthquakes: Large aftershocks outside the classical aftershock zone, J. Geophys. Res. Solid Earth, 107, ESE-9, https://doi.org/10.1029/2001JB000646, 2002.

Peláez, J. A., Henares, J., Hamdache, M., and Sanz de Galdeano, C.: A Seismogenic Zone Model for Seismic Hazard Studies in Northwestern Africa, 643–680, https://doi.org/10.1007/978-3-319-77359-9_29, 2018.

Perea, H., Gràcia, E., Alfaro, P., Bartolomé, R., Iacono, C. Lo, Moreno, X., Masana, E., and Team, E.-S.: Quaternary active tectonic structures in the offshore Bajo Segura basin (SE Iberian Peninsula–Mediterranean Sea), Nat. Hazards Earth Syst. Sci., 12, 3151–3168, https://doi.org/10.5194/nhess-12-3151-2012, 2012.

Perea, H., Gràcia, E., Martínez-Loriente, S., Bartolome, R., de la Peña, L. G., de Mol, B., Moreno, X., Iacono, C. Lo, Diez, S., Tello, O., Gómez-Ballesteros, M., and Dañobeitia, J. J.: Kinematic analysis of secondary faults within a distributed shear-zone reveals fault linkage and increased seismic hazard, Mar. Geol., 399, 23–33, https://doi.org/10.1016/j.margeo.2018.02.002, 2018.

Platt, J. P. and Vissers, R. L. M.: Extensional collapse of thickened continental lithosphere: a working hypothesis for the Alboran Sea and Gibraltar arc, Geology, 17, 540–543, https://doi.org/10.1130/0091-7613(1989)017<0540:ECOTCL>2.3.CO;2, 1989.

Platt, J. P., Behr, W. M., Johanesen, K., and Williams, J. R.: The Betic-Rif arc and its orogenic hinterland: A review, Annu. Rev. Earth Planet. Sci., 41, 313–357, https://doi.org/10.1146/annurev-earth-050212-123951, 2013.

Plimmer, A.: Constraining the relationship between mantle circulation and supercontinent cycles, 2025.

Porkoláb, K.: Burial-exhumation cycles in the continental crust derived from Mediterranean field studies and numerical modelling, https://doi.org/10.33540/737, 2021.

Poujol, A., Ritz, J.-F., Tahayt, A., Vernant, P., Condomines, M., Blard, P.-H., Billant, J., Vacher, L., Tibari, B., and Hni, L.: Active tectonics of the Northern Rif (Morocco) from geomorphic and geochronological data, J. Geodyn., 77, 70–88, https://doi.org/10.1016/j.jog.2014.01.004, 2014.

Prejean, S., Ellsworth, W., Zoback, M., and Waldhauser, F.: Fault structure and kinematics of the Long Valley Caldera region, California, revealed by high-accuracy earthquake hypocenters and focal mechanism stress inversions, J. Geophys. Res. Solid Earth, 107, ESE-9, https://doi.org/10.1029/2001jb001168, 2002.

Rebaï, S., Philip, H., and Taboada, A.: Modern tectonic stress field in the Mediterranean region: evidence for variation in stress directions at different scales, Geophys. J. Int., 110, 106–140, https://doi.org/10.1111/j.1365-246X.1992.tb00717.x, 1992.

Ross, Z. E., Cochran, E. S., Trugman, D. T., and Smith, J. D.: 3D fault architecture controls the dynamism of earthquake swarms, Science (80-.)., 368, 1357–1361, https://doi.org/10.1126/science.abb0779, 2020.

Ryan, K. J. and Oglesby, D. D.: Dynamically modeling fault step overs using various friction laws, J. Geophys. Res. Solid Earth, 119, 5814–5829, https://doi.org/10.1002/2014JB011151, 2014.

Sanz de Galdeano, C., Azañón, J. M., Cabral, J., Ruano, P., Alfaro, P., Canora, C., Ferrater, M., García Tortosa, F. J., García-Mayordomo, J., and Gràcia, E.: Active faults in Iberia, Geol. Iberia A Geodyn. approach Vol. 5 Act. Process. Seism. Act. faulting Reli., 33–75, https://doi.org/10.1007/978-3-030-10931-8_4, 2019.

Saunders, A. D., Jones, S. M., Morgan, L. A., Pierce, K. L., Widdowson, M., and Xu, Y. G.: Regional uplift associated with continental large igneous provinces: The roles of mantle plumes and the lithosphere, Chem. Geol., 241, 282–318, https://doi.org/10.1016/j.chemgeo.2007.01.017, 2007.

https://doi.org/10.5194/egusphere-2025-6433
Preprint. Discussion started: 21 April 2026

Schaff, D. P. and Richards, P. G.: Repeating seismic events in China, Science (80-.)., 303, 1176–1178, https://doi.org/10.1126/science.1093422, 2004.

Schaff, D. P. and Waldhauser, F.: Waveform cross-correlation-based differential travel-time measurements at the Northern California Seismic Network, Bull. Seismol. Soc. Am., 95, 2446–2461, https://doi.org/10.1785/0120040221, 2005.

Seber, D., Barazangi, M., Ibenbrahim, A., and Demnati, A.: Geophysical evidence for lithospheric delamination beneath the alboran sea and rif-betic mountains, Nature, 379, 785–790, https://doi.org/10.1038/379785a0, 1996.

Serpelloni, E., Vannucci, G., Pondrelli, S., Argnani, A., Casula, G., Anzidei, M., Baldi, P., and Gasperini, P.: Kinematics of the Western Africa-Eurasia plate boundary from focal mechanisms and GPS data, Geophys. J. Int., 169, 1180–1200, https://doi.org/10.1111/j.1365-246X.2007.03367.x, 2007.

Shapiro, S. A. and Dinske, C.: Fluid-induced seismicity: Pressure diffusion and hydraulic fracturing, Geophys. Prospect., 57, 301–310, https://doi.org/10.1111/j.1365-2478.2008.00770.x, 2009.

Shapiro, S. A., Huenges, E., and Borm, G.: Estimating the crust permeability from fluid-injection-induced seismic emission at the KTB site, Geophys. J. Int., 131, F15–F18, https://doi.org/10.1111/j.1365-246X.1997.tb01215.x, 1997.

Shelly, D. R.: Examining the connections between earthquake swarms, crustal fluids, and large earthquakes in the context of the 2020–2024 Noto Peninsula, Japan, Earthquake sequence, Geophys. Res. Lett., 51, e2023GL107897, https://doi.org/10.1029/2023GL107897, 2024.

Shelly, D. R., Beroza, G. C., and Ide, S.: Complex evolution of transient slip derived from precise tremor locations in western Shikoku, Japan, Geochemistry, Geophys. Geosystems, 8, https://doi.org/10.1029/2007GC001640, 2007.

Shelly, D. R., Hill, D. P., Massin, F., Farrell, J., Smith, R. B., and Taira, T.: A fluid-driven earthquake swarm on the margin of the Yellowstone caldera, J. Geophys. Res. Planets, 118, 4872–4886, https://doi.org/10.1002/jgrb.50362, 2013.

Shelly, D. R., Taira, T., Prejean, S. G., Hill, D. P., and Dreger, D. S.: Fluid-faulting interactions: Fracture-mesh and fault-valve behavior in the February 2014 Mammoth Mountain, California, earthquake swarm, Geophys. Res. Lett., 42, 5803–5812, https://doi.org/10.1002/2015GL064325, 2015.

Sibson, R. H.: Fault-valve behavior and the hydrostatic-lithostatic fluid pressure interface, Earth-Science Rev., 32, 141–144, https://doi.org/10.1016/0012-8252(92)90019-P, 1992.

Sibson, R. H.: Structural permeability of fluid-driven fault-fracture meshes, J. Struct. Geol., 18, 1031–1042, https://doi.org/10.1016/0191-8141(96)00032-6, 1996.

Somoza, L., Medialdea, T., Terrinha, P., Ramos, A., and Vázquez, J.-T.: Submarine active faults and Morpho-Tectonics around the Iberian margins: seismic and tsunamis hazards, Front. Earth Sci., 9, 653639, https://doi.org/10.3389/feart.2021.653639, 2021.

Soumaya, A., Ben Ayed, N., Rajabi, M., Meghraoui, M., Delvaux, D., Kadri, A., Ziegler, M., Maouche, S., and Braham, A.: Active faulting geometry and stress pattern near complex strike-slip systems along the Maghreb region: Constraints on active convergence in the Western Mediterranean, Tectonics, 37, 3148–3173, https://doi.org/10.1029/2018TC004983, 2018.

Spakman, W. and Wortel, R.: A tomographic view on western Mediterranean geodynamics, in: The TRANSMED atlas. The Mediterranean region from crust to mantle, Springer, 31–52, https://doi.org/10.1007/978-3-642-18919-7_2, 2004.

Stich, D., Mancilla, F. de L., Baumont, D., and Morales, J.: Source analysis of the Mw 6.3 2004 Al Hoceima earthquake (Morocco) using regional apparent source time functions, J. Geophys. Res. Solid Earth, 110, https://doi.org/10.1029/2004JB003366, 2005.

Stich, D., Martín, R., and Morales, J.: Moment tensor inversion for Iberia–Maghreb earthquakes 2005–2008, Tectonophysics, 483, 390–398, https://doi.org/10.1016/j.tecto.2009.11.006, 2010.

Stich, D., Martín, R., Morales, J., López-Comino, J. Á., and Mancilla, F. de L.: Slip Partitioning in the 2016 Alboran Sea Earthquake Sequence (Western Mediterranean), Front. Earth Sci., 8, 587356, https://doi.org/10.3389/feart.2020.587356, 2020.

Tachema, A., Nadji, A., and Sondhiya, D. K.: Space-based GNSS radio signals to investigate ionospheric plasma changes

https://doi.org/10.5194/egusphere-2025-6433
Preprint. Discussion started: 21 April 2026

preceding the 2016 Al Hoceima-Morocco earthquake, Mw= 6.4, Ann. Geophys., 66, SE643–SE643, https://doi.org/10.4401/ag-8901, 2023.

Tahayt, A., Mourabit, T., Rigo, A., Feigl, K. L., Fadil, A., McClusky, S., Reilinger, R., Serroukh, M., Ouazzani-Touhami, A., Sari, D. Ben, and Vernant, P.: Mouvements actuels des blocs tectoniques dans l'arc Bético-Rifain à partir des mesures GPS entre 1999 et 2005, Comptes Rendus - Geosci., 340, 400–413, https://doi.org/10.1016/j.crte.2008.02.003, 2008a.

Tahayt, A., Mourabit, T., Rigo, A., Feigl, K. L., Fadil, A., McClusky, S., Reilinger, R., Serroukh, M., Ouazzani-Touhami, A., and Sari, D. Ben: Present-day movements of tectonic blocks in the Betic-Rif Arc from GPS measurements 1999-2005, Contrib. to Mineral. Petrol., 340, 400–413, https://doi.org/10.1016/j.crte.2008.02.003, 2008b.

Tahayt, A., Feigl, K. L., Mourabit, T., Rigo, A., Reilinger, R., McClusky, S., Fadil, A., Berthier, E., Dorbath, L., and Serroukh, M.: The Al Hoceima (Morocco) earthquake of 24 February 2004, analysis and interpretation of data from ENVISAT ASAR and SPOT5 validated by ground-based observations, Remote Sens. Environ., 113, 306–316, https://doi.org/10.1016/j.rse.2008.09.015, 2009.

Tendero-Salmerón, V., Lafosse, M., D'acremont, E., Rabaute, A., Azzouz, O., Ercilla, G., Makkaoui, M., and Galindo-Zaldivar, J.: Application of Automated Throw Backstripping Method to Characterize Recent Faulting Activity Migration in the Al Hoceima Bay (Northeast Morocco): Geodynamic Implications, Front. Earth Sci., 233, https://doi.org/10.3389/feart.2021.645942, 2021.

Tendero-Salmerón, V., Galindo-Zaldivar, J., d'Acremont, E., Catalán, M., Martos, Y. M., Ammar, A., and Ercilla, G.: New insights on the Alboran Sea basin extension and continental collision from magnetic anomalies related to magmatism (western Mediterranean), Mar. Geol., 443, 106696, https://doi.org/10.1016/j.margeo.2021.106696, 2022.

Thurner, S., Palomeras, I., Levander, A., Carbonell, R., and Lee, C.: Ongoing lithospheric removal in the western Mediterranean: evidence from Ps receiver functions and thermobarometry of Neogene basalts (PICASSO project), Geochemistry, Geophys. Geosystems, 15, 1113–1127, https://doi.org/10.1002/2013GC005124, 2014.

Tormann, T., Wiemer, S., and Mignan, A.: Systematic survey of high-resolution b value imaging along Californian faults: Inference on asperities, J. Geophys. Res. Solid Earth, 119, 2029–2054, https://doi.org/10.1002/2013JB010867, 2014.

Torne, M., Fernàndez, M., Comas, M. C., and Soto, J. I.: Lithospheric structure beneath the Alboran Basin: Results from 3D gravity modeling and tectonic relevance, J. Geophys. Res. Solid Earth, 105, 3209–3228, https://doi.org/10.1029/1999jb900281, 2000.

Uchida, N. and Bürgmann, R.: Repeating Earthquakes, Annu. Rev. Earth Planet. Sci., 47, 305–332, https://doi.org/10.1146/annurev-earth-053018-060119, 2019.

Vernant, P., Fadil, A., Mourabit, T., Ouazar, D., Koulali, A., Davila, J. M., Garate, J., McClusky, S., and Reilinger, R.: Geodetic constraints on active tectonics of the Western Mediterranean: Implications for the kinematics and dynamics of the Nubia-Eurasia plate boundary zone, J. Geodyn., 49, 123–129, https://doi.org/10.1016/j.jog.2009.10.007, 2010.

Vidale, J. E. and Shearer, P. M.: A survey of 71 earthquake bursts across southern California: Exploring the role of pore fluid pressure fluctuations and aseismic slip as drivers, J. Geophys. Res. Solid Earth, 111, https://doi.org/10.1029/2005JB004034, 2006.

Vidil, L., D'Acremont, E., Emmanuel, L., Lafuerza, S., Caroir, F., Leroy, S., Latni, E. M., and Rabaute, A.: Late Quaternary fault activity of the southern part of the Al Idrissi strike-slip fault system, Alboran sea: an integrated multi-proxy approach, in: EGU General Assembly 2025, https://doi.org/10.5194/egusphere-egu25-13085, 2025a.

Vidil, L., D'Acremont, E., Emmanuel, L., Caroir, F., Lafuerza, S., Leroy, S., Ercilla, G., Rabaute, A., Galindo-Zaldivar, J., Latni, E. M., Guittet, A., and Brouillet, J. F.: Multi-proxy investigations into the active tectonics of the Bokkoya strike-slip fault, southern Alboran Sea, Tectonophysics, 915, 230922, https://doi.org/10.1016/j.tecto.2025.230922, 2025b.

Villaseñor, A., Chevrot, S., Harnafi, M., Gallart, J., Pazos, A., Serrano, I., Córdoba, D., Pulgar, J. A., and Ibarra, P.: Subduction and volcanism in the Iberia-North Africa collision zone from tomographic images of the upper mantle, Tectonophysics, 663,

https://doi.org/10.5194/egusphere-2025-6433
Preprint. Discussion started: 21 April 2026

238–249, https://doi.org/10.1016/j.tecto.2015.08.042, 2015.

Waldhauser, F.: hypoDD—A Program to Compute Double-Difference Hypocenter Locations: U.S. Geological Survey Open-File Report, Https://Pubs.Usgs.Gov/of/2001/0113/, 25 pp., 2001.

Waldhauser, F. and Ellsworth, W. L.: A double-difference earthquake location algorithm: Method and application to the northern Hayward fault, California, Bull. Seismol. Soc. Am., 90, 1353–1368, https://doi.org/10.1785/0120000006, 2000.

Wallace, P. J.: Volatiles in subduction zone magmas: Concentrations and fluxes based on melt inclusion and volcanic gas data, J. Volcanol. Geotherm. Res., 140, 217–240, https://doi.org/10.1016/j.jvolgeores.2004.07.023, 2005.

Wiemer, S. and Wyss, M.: Minimum magnitude of completeness in earthquake catalogs: Examples from Alaska, the Western United States, and Japan, Bull. Seismol. Soc. Am., 90, 859–869, https://doi.org/10.1785/0119990114, 2000.

Zelenin, E., Bachmanov, D., Garipova, S., Trifonov, V., and Kozhurin, A.: The Active Faults of Eurasia Database (AFEAD): the ontology and design behind the continental-scale dataset, Earth Syst. Sci. Data, 14, 4489–4503, https://doi.org/10.5194/essd-14-4489-2022, 2022.

Zhang, H. and Thurber, C. H.: Double-difference tomography: The method and its application to the Hayward fault, California, Bull. Seismol. Soc. Am., 93, 1875–1889, https://doi.org/10.1785/0120020190, 2003.

Zhou, Z., Yu, N., Wang, T., Kong, W., Chen, H., and Li, T.: Episodic earthquakes controlled by the migration of crustal fluids and fault valve behavior, Geophys. Res. Lett., 52, e2024GL114093, https://doi.org/10.1029/2024GL114093, 2025.

Zhu, W., Allison, K. L., Dunham, E. M., and Yang, Y.: Fault valving and pore pressure evolution in simulations of earthquake sequences and aseismic slip, Nat. Commun., 11, 4833, https://doi.org/10.1038/s41467-020-18598-z, 2020.